NISTIR 5113

Proton Monte Carlo Transport Program PTRAN

Martin J. Berger

U.S. DEPARTMENT OF COMMERCE
Technology Administration
National Institute of Standards
and Technology
Physics Laboratory
Ionizing Radiation Division
Gaithersburg, MD 20899

Prepared for:

National Cancer Institute
Bethesda, MD 20892

NIST

NISTIR 5113

Proton Monte Carlo Transport Program PTRAN

Martin J. Berger

U.S. DEPARTMENT OF COMMERCE
Technology Administration
National Institute of Standards
and Technology
Physics Laboratory
Ionizing Radiation Division
Gaithersburg, MD 20899

Prepared for:

National Cancer Institute
Bethesda, MD 20892

January 1993

U.S. DEPARTMENT OF COMMERCE
Barbara Hackman Franklin, Secretary

TECHNOLOGY ADMINISTRATION
Robert M. White, Under Secretary for Technology

NATIONAL INSTITUTE OF STANDARDS
AND TECHNOLOGY
John W. Lyons, Director

PROTON MONTE CARLO TRANSPORT PROGRAM PTRAN

Martin J. Berger*

National Institute of Standards and Technology
Gaithersburg, MD 20899, USA

ABSTRACT

This report describes the structure and use of Monte Carlo programs that calculate the transport of proton beams through extended media. Although more generally applicable, the programs have been designed to deal with the penetration of 50- to 250-MeV beams through water phantoms. The Monte Carlo model takes into account multiple-scattering deflections and energy-loss straggling due to Coulomb interactions of protons with atoms and orbital electrons. Nonelastic nuclear interactions are treated as an absorptive effect. The PTRAN system at present consists of several cross-section preparation programs and two main codes, PTRAN3D and PTRAN1D. PTRAN3D applies to an incident narrow pencil beam, and calculates (a) the deposition of energy as function of depth and radial distance from the beam axis, and (b) and the energy spectra of the primary protons as function of depth. Program PTRAN1D is a simplified version which runs faster and omits the calculation of the radial distribution of energy deposition.

*Contractor, work done under NIST contract 50SBN2C7042.

1. Introduction

This report describes a system of Monte Carlo programs for calculating the penetration, diffusion and slowing down of proton beams in an extended, homogeneous medium. The objective is to provide information useful for treatment planning and dosimetry in proton therapy. Attention is therefore focussed on the penetration through water of proton beams with initial energies from 50 MeV to 250 MeV.

The Monte Carlo model is based on the condensed-random-walk method (Berger, 1963), and takes into account the following types of events occurring in successive short track segments: (a) energy-loss straggling in Coulomb collisions with atomic electrons, (b) multiple-scattering deflections due to elastic scattering by atoms, and (c) energy losses in nonelastic nuclear reactions. The Monte Carlo model can be applied to a variety of transport problems. In this report, programs are described which calculate the spatial distribution of energy deposition (in one or three dimensions), as well as energy spectra of protons at various depths in a phantom.

In Section 2, procedures for the simulation of proton tracks are described. In Section 3, data preparation programs are described which facilitate the sampling of energy losses from the distribution of Vavilov (1957) and the sampling of angular deflections from the distribution of Molière (1948). With these procedures one can construct Monte Carlo programs for treating a variety of proton transport problems. Two such programs are described in this report. Section 4 deals with program PTRAN3D, which calculates the deposition of energy as function of depth and of the radial distance from a narrow pencil beam, and also proton spectra as functions of depth. Section 5 describes a simpler one-dimensional program PTRAN1D, which omits the calculation of the radial energy-deposition distribution. Section 6 discusses the random-number generators used in the PTRAN programs. Section 7 provides information about the dependence of the results on the step-size of the condensed-random walk model. In Section 8, the program and data files are listed which are included in the PTRAN system at the present time.

For the purpose of calculating the spatial distribution of energy deposition, the transfer of energy from the proton beam to the medium can be treated as a two-stage process. In the important first stage one considers the spatial distribution of (1) proton energy losses that occur as the result of Coulomb interactions with atoms or molecules, and (2) of the removal of protons from the beam due to nonelastic nuclear interactions. In the second stage one takes into account the further spatial transport of energy by secondary electrons from ionization events, and by charged particles, neutrons, or gamma rays from nuclear reactions. The Monte Carlo programs described in this report deal only with the first stage.

The ranges of the secondary electrons are exceedingly short compared to the ranges of the primary protons. Therefore energy transport by secondary electrons has an effect on depth dose curves only at very shallow depths, where it gives rise to a rapid dose buildup. In regard to nonelastic nuclear reactions, one must estimate the fraction of the energy lost by protons that escape in the form of neutrons, x-rays, or fast protons, and the fraction that can be considered to be absorbed locally. It is also of interest to calculate the energy degradation spectra of the secondary heavy charged particles. Work on these topics is in progress at NIST by S. M. Seltzer, and the results will be integrated into the analysis of output from the PTRAN codes.

2. Monte Carlo Model

2.1. Schematization.

For the purpose of simulation, proton tracks are divided into many short segments. These segments are also called the "steps" of a condensed random walk. Energy-losses in successive steps are sampled from the Vavilov distribution (Vavilov, 1957). The multiple-scattering angular deflection in successive steps are sampled from the Molière distribution (Molière, 1948). Nonelastic nuclear reactions are treated an absorptive effect. Appendices 1 and 2 list the formulas used for calculating the Molière and Vavilov distributions.

In condensed-random-walk model used in the present work, a proton track (Monte Carlo history) is described by the following array:

$$\begin{array}{llllll} s_0, & s_1, & s_2, & \ldots., & s_n, & \ldots \\ E_0, & E_1, & E_2, & \ldots., & E_n, & \ldots \\ x_0, & x_1, & x_2, & \ldots., & x_n, & \ldots \\ y_0, & y_1, & y_2, & \ldots., & y_n, & \ldots \\ z_0, & z_1, & z_2, & \ldots., & z_n, & \ldots \\ \theta_0, & \theta_1, & \theta_2, & \ldots., & \theta_n, & \ldots \\ \varphi_0, & \varphi_1, & \varphi_2, & \ldots., & \varphi_n, & \ldots \\ W_0, & W_1, & W_2, & \ldots., & W_n, & \ldots \end{array} \qquad (2.1)$$

The index n pertains to the track characteristics at the end of the n^{th} step. s_n is the path length traveled by the proton since its entry into the medium, and $\Delta s_n = s_{n+1} - s_n$ is the size of the n^{th} step. E_n is the kinetic energy; x_n, y_n and z_n are spatial coordinates; θ_n and φ_n specify the direction of motion in a spherical coordinate system whose polar axis is the z-axis; W_n is a survival weight factor which represents the probability that the proton has not been absorbed, in path length s_n, by a nonelastic nuclear reaction. The index 0 pertains to the initial conditions, at the point of entry of the proton into the medium, so that $s_0 = 0$ and $W_0 = 1$.

2.2. Choice of Step Sizes.

Several considerations enter into the choice of the step sizes of the condensed random walk. In order to reduce the computing time, the steps should be as large as possible. In order to reduce the error resulting from the neglect of individual collisions, the steps should be as short as possible. The steps must be sufficiently long so that the Vavilov energy-loss distribution and Molière multiple-scattering distribution are both applicable. On the other hand, the steps should be short enough so that the energy loss per step is a small fraction of the proton energy at the beginning of the step.

In the implementation of the condensed random walk model in the PTRAN system, the choice of step sizes is made via the adoption of an energy grid at which the various cross sections and probability distributions are evaluated. This arrangement will be discussed in Section 3.1. Some numerical experiments were carried out to explore the effects of changing the step sizes, and will be discussed in Section 7.

2.3. Energy Loss and Change of Direction.

The energy loss in the n^{th} step, $E_n - E_{n+1}$, is sampled from the Vavilov distribution. The multiple-scattering angular deflection in the n^{th} step is specified in terms of two angles, θ' and φ', in a coordinate system whose polar axis coincides with the direction of motion of the proton at the beginning of the segment. The angle θ' is sampled from the Molière distribution, and the azimuthal angle φ' from a uniform distribution between -180 and 180 degrees. The direction cosines of the proton track at the end of the n^{th} step are given by

$$\begin{bmatrix} \sin\theta_{n+1}\cos\varphi_{n+1} \\ \sin\theta_{n+1}\sin\varphi_{n+1} \\ \cos\theta_{n+1} \end{bmatrix} = R \cdot \begin{bmatrix} \sin\theta'\cos\varphi' \\ \sin\theta'\sin\varphi' \\ \cos\theta' \end{bmatrix} , \tag{2.2}$$

where R is the rotation matrix

$$R = \begin{bmatrix} \cos\theta_n\cos\varphi_n & -\sin\varphi_n & \sin\theta_n\cos\varphi_n \\ \cos\theta_n\sin\varphi_n & \cos\varphi_n & \sin\theta_n\sin\varphi_n \\ -\sin\theta_n & 0 & \cos\theta_n \end{bmatrix} . \tag{2.3}$$

In the PTRAN codes, Eqs (2.2) and (2.3) are replaced by the equivalent equations

$$\cos\theta_{n+1} = \cos\theta_n\cos\theta' - \sin\theta_n\sin\theta'\cos\varphi' , \tag{2.4}$$

$$\sin(\varphi_{n+1} - \varphi_n) = \frac{\sin\theta'\sin\varphi'}{\sin\theta_{n+1}} , \tag{2.5}$$

$$\cos(\varphi_{n+1} - \varphi_n) = \frac{\cos\theta' - \cos\theta_n\cos\theta_{n+1}}{\sin\theta_n\sin\theta_{n+1}} . \tag{2.6}$$

When $\sin\theta_n \sin\theta_{n+1} = 0$, then $\varphi_{n+1} - \varphi_n = \varphi'$.

2.4. Change of Position.

Let $\Delta x'$, $\Delta y'$, and $\Delta z'$ denote the spatial displacements or the proton in the n^{th} step, in a Cartesian coordinate system whose axis coincides with the direction of motion at the beginning of the step. Taking into account multiple scattering, these displacements are calculated from the following approximate expressions:

$$\Delta x' = \frac{1}{2}\,\Delta s_n \left[\sin\theta' \cos\varphi' + k_x\,(\overline{\theta^2}/6)^{1/2}\right] \tag{2.7}$$

$$\Delta y' = \frac{1}{2}\,\Delta s_n \left[\sin\theta' \sin\varphi' + k_y\,(\overline{\theta^2}/6)^{1/2}\right] \tag{2.8}$$

$$\Delta z' = \frac{1}{2}\,\Delta s_n\,(1 + \cos\theta') \quad . \tag{2.9}$$

Here θ' and φ' are the multiple-scattering angular deflections, and k_x and k_y are random variables distributed according to a Gaussian distribution with zero mean and unit standard deviation. The quantity $\overline{\theta^2}$ is the mean-square multiple-scattering deflection which is approximated by $\chi_c^2(B-1.2)$, where χ_c^2 and B are variables in Molière's multiple-scattering theory (see Appendix 1).

The corresponding spatial displacements in a fixed coordinate system are related to $\Delta x'$, $\Delta y'$, and $\Delta z'$ by the rotation matrix R from Eq (2.3):

$$\begin{bmatrix} x_{n+1} - x_n \\ y_{n+1} - y_n \\ z_{n+1} - z_n \end{bmatrix} = R \cdot \begin{bmatrix} \Delta x' \\ \Delta y' \\ \Delta z' \end{bmatrix} \quad . \tag{2.10}$$

2.5. Nuclear Survival Weights.

The weight factor W_n is treated in PTRAN on the basis of the continuous-slowing-down approximation, assuming that

$$W_n(T) = \exp\left[-\int_T^{T_0} \mu_{nuc}(T')\,\frac{dT'}{S(T')}\right] \quad , \tag{2.11}$$

where μ_{nuc} is a nuclear absorption coefficient that represents the probability, per unit path length, of a nonelastic nuclear reaction. This coefficient is given by

$$\mu_{nuc}(T) = \frac{N_{av}}{A}\,\sigma(T) \quad , \tag{2.12}$$

where N_{av} is Avogadro's number, A the molecular weight, and σ the total non-elastic nuclear reaction cross section.

3. Data Preparation Programs

Proton stopping powers and ranges were calculated with the program PSTAR (Berger, 1992) which generates results consistent with those tabulated in Report 49 of the International Commission on Radiation Units and Measurements (ICRU, 1992). Stopping powers and ranges in water are given in table 1.

The nonelastic nuclear cross section for hydrogen is negligible. The adopted cross section for oxygen, shown in figure 1, is based on a fit to experimental results of Renberg *et al.* (1972) and Carlson *et al.* (1975). In the energy region from threshold up to 10 MeV the energy-dependence of the adopted cross section is modeled after theoretical results (S. M. Seltzer, private communication) obtained with the GNASH code of Young *et al.* (1990).

3.1. Program PARAM4.

A sequence of decreasing energies T_0, T_1, T_2, ..., T_m, ..., T_M is chosen such that the difference $T_m - T_{m+1}$ has either a constant value ΔT, or the value kT_m, whichever is smaller. In the exploratory calculations described in this report, five such energy grids were used, with $\Delta T = 4$, 2, 1, 0.5 and 0.25 MeV, and with $k = 0.05$ in all cases.

For each energy interval (T_m, T_{m+1}), a path length δs_m, is calculated in the continuous-slowing-down approximation:

$$\delta s_m = r_0(T_m) - r_0(T_{m+1}) = \int_{T_{m+1}}^{T_m} \frac{dT}{S(T)} \quad , \tag{3.1}$$

where S(T) is the stopping power. The set of path lengths δs_m, $m = 1, \ldots, M$, will be referred to as a step-size grid. Actual step-sizes are chosen in the PTRAN programs by interpolation in a table of δs_m *vs.* T_m.

Various parameters of the Molière and Vavilov distribution are calculated in PARAM4 for path lengths δs_m, using the formulas in Appendices 1 and 2. The Vavilov parameters are evaluated for an initial energy T_m. The Molière parameters are evaluated at an intermediate energy $(T_m + T_{m+1})/2$, in order to account for the energy loss along the track. PARAM4 also tabulates the values of the proton stopping power and range, the nuclear attenuation coefficient, and the survival weight factor W, at energy T_m.

Input Parameters. The user is prompted to provide, from the keyboard, the grid parameters ΔT and k, and the starting energy T_0 and length M of the grid. On the monitor screen it is indicated how these quantities can be chosen to obtain the five grids mentioned above. The user is free, however, to make different choices. The user must also specify the names of the output files, and suggested names are supplied.

Input Data Files. The following files are required:

COMPOS.WAT	Composition data for water
STOPRANG.WAT	Stopping power and range table for water
OXFIT.DAT	Cross section for non-elastic reactions of protons with oxygen nuclei

PARAM4 could be adapted to materials other than water. Small modifications of the source code would be necessary, which are indicated in the program listing.

Output from PARAM4: Three output files are generated:

1) Output table for inspection by the user, with a suggested name PARAM4.TBj, where j identifies the step-size grid.

2) A file of data to be used as input for programs VPREP4 and MPREP4, with the suggested name PARAM4.ARj.

3) A file of data to be used as input to the main Monte Carlo program (such as PTRAN1D or PTRAN3D), with the suggested name PARAM4.PTj.

Output table PARAM4.TBj lists various quantities pertaining to the Molière and Vavilov distributions, as well as nuclear attenuation coefficients and survival factors. By inspecting this table, the user can determine, for example, whether the values of the Molière parameter B, as required, are greater 4.5; or whether the values of the Vavilov parameter are, as required, much larger than the mean excitation energy of the medium. An excerpt from output file PARAM4.TB4, for Grid 4, is shown in table 2.

3.2. Program VPREP4 and Related Programs.

Arrays for Alias Sampling Method. In PTRAN, energy losses are sampled from the Vavilov distribution by a two-step procedure. First, a random selection is made of a bin in a histogram of the Vavilov distribution, and then a value of the scaled energy loss is chosen at random within this bin.

VPREP4 calculates the Vavilov distribution $F_V(\lambda,\beta,\kappa)$ according to Eq (A2.6) as a function of the scaled energy-loss variable λ, the proton velocity β and the skewness parameter κ (see Appendix 2). The integral in Eq (A2.6) is evaluated by an adaptive numerical quadrature code (Kahaner *et al.*, 1989). The distribution is then converted into a histogram with a constant bin width $\Delta\lambda = 0.1$.

The random selection of a histogram bin is done by the alias sampling method (Walker, 1974; Kronmal and Peterson, 1979), which has the advantage that a single random number and a single comparison are sufficient. VPREP4 calculates, from the Vavilov histogram, two auxiliary arrays which are required by the alias sampling method. This is done with subroutine ALIAS which is an adaptation of a program developed by Kronmal and Peterson (private communication).

Output Options. There are two options, one for production and the other one for testing:

1) *Output for use in PTRAN programs*. The arrays needed for the alias sampling method are calculated for many grid intervals between specified lower and upper limits. The output is stored in a large formatted file with the suggested name VPREP4.ARj, where j indicates the grid. In order to reduce the time needed to enter these data into the PTRAN programs, a conversion program VCON4 is used to generate from VPREP4.ARj a corresponding binary file with the suggested name VPREP4.BRj. Such a file can provide input for Monte Carlo calculations involving proton beams with many different energies.

2) *Output for Testing*. The output file contains the two alias-method arrays, and the underlying probability histogram, for a single grid interval. These data can be used as input for an auxiliary program called VSAMP4, which samples energy losses by the alias method. The sampled histogram can be compared with probability histogram to verify that the sampling procedure works correctly.

With this option it is also possible to generate an output file which contains the Vavilov distribution (rather than a histogram) as a function of the scaled energy-loss parameter λ. Vavilov distributions for grid intervals with starting energies $T_m = 25$, 50, 100 and 200 MeV (for Grid 4) are illustrated in figure 2. Program VSUM4 uses numerical quadrature to obtain the mean value and variance of the Vavilov distribution. This allows the user to check that the mean value equals $T_m - T_{m+1}$, and that the variance equals the theoretical variance from Eq (A2.13). Finally, with option 2 it is also possible to omit the Blunck-Leisegang correction, setting $\epsilon = 0$ in Eq (A2.8) of Appendix 2. For the grids used in this paper, this omission would have very little effect on the calculated Vavilov distributions.

3.3. Program MPREP4 and Related Programs.

MPREP4 calculates the Molière distribution for each path length δs_m, using the equations in Appendix 1. The distribution is evaluated at 156 values (between 0 and 40) of the reduced Molière angle ϑ. The spacing of the angles is non-uniform, and increases with increasing ϑ. The set of ϑ-values is contained in file THSET2. A probability histogram with 155 non-uniform bins is then calculated, and is used to obtain the two auxiliary arrays for the alias sampling method. There are two output options:

1) *Output for use in PTRAN programs*. The output file contains the two arrays for the alias sampling method, for the entire grid. The output file is a large formatted file with the suggested name MPREP4.ARj. Program MCON4 is used to generate a corresponding unformatted (binary) file MPREP4.BRj.

2) *Output for Testing*. The output includes the two alias method arrays, and the underlying probability histogram, for a single grid interval. These data can be used as input for an auxiliary program MSAMP4, which samples angular deflections by the alias method. The sampled histogram can be compared with input probability histogram, to verify that the sampling procedure works correctly.

4. Monte Carlo Program PTRAN3D

4.1. Statement of the Problem.

A homogeneous, laterally unbounded medium is assumed to occupy the region $z \geq 0$. A narrow monoenergetic pencil beam of protons is assumed to be incident along the z-axis. The information sought includes:

(1) dE/dz, the average rate of energy loss by the proton beam per unit depth, as a function of the depth z. The units of dE/dz are MeV cm^2/g. Actually two such quantities are calculated:

$(dE/dz)_c$, pertaining to energy losses that result from Coulomb interactions with atoms,

$(dE/dz)_n$, pertaining to energy losses that result from non-elastic interactions with nuclei.

(2) y(T,z), the proton energy spectrum, expressed in terms of the average track length per unit depth and per unit energy, as a function of the proton energy T and the depth z. The units are MeV^{-1}.

(3) $f(\rho,z)$, the radial distribution of the energy lost by the proton beam (in Coulomb interactions), as a function of the distance ρ from z axis.

Because of the short range of the secondary electrons, it is a very good approximation to consider the quantity $(dE/dz)_c$ equal to the energy deposition per unit depth due to Coulomb interactions, $(dD/dz)_c$. As will be shown in a later report, the energy deposition per unit depth due to nuclear interactions, $(dD/dz)_n$, is approximately equal to 0.6 $(dE/dz)_n$. The discount factor 0.6 arises mainly from the fact that a large fraction of the energy used for nuclear reactions eventually escapes in the form of penetrating secondary neutrons.

Also computed by PTRAN3D are the mean energy $T_{av}(z)$ and the standard deviation $\sigma_T(z)$, which are evaluated as track averages:

$$T_{av}(z) = \frac{\int_0^{T_0} T\, y(T,z)\, dT}{\int_0^{T_0} y(T,z)\, dT} \tag{4.1.1}$$

$$\sigma_T^2(z) = \frac{\int_0^{T_0} (T - T_{av})^2\, y(T,z)\, dT}{\int_0^{T_0} y(T,z)\, dT} \,. \tag{4.1.2}$$

4.2. Track Simulation.

The simulation of proton tracks is based on the procedures outlined in Section 2, and uses the data sets generated by programs VPREP4 and MPREP4. Suppose the proton has reached energy E, and the events in the n^{th} step are to be sampled. The step size Δs_n is obtained by interpolating to energy E in the table of δs_m *vs* T_m. The grid index m is calculated such that T_m is the closest grid energy to E. The scaled energy loss λ is sampled from the Vavilov distribution, and the scaled deflection angle ϑ from the Molière distribution, using the alias-method arrays for grid interval (T_m, T_{m+1}). The use of pre-computed distributions for this grid interval, instead of a distribution for an initial energy E and path length Δs_n, is an approximation which speeds up the calculation. The error incurred thereby is very small because the variation with energy of the scaled distributions is very slow. From the scaled energy loss λ, the actual energy loss $E_n - E_{n+1}$ is determined according to Eqs (A2.1) and (A2.4) of Appendix 2, using $\Delta_{av} = T_m - T_{m+1}$, and values of ξ and λ_{av} interpolated to energy E. The multiple scattering deflection angle θ' is determined from ϑ according to Eq (A1.2) of Appendix 1, using a value of $\chi_c B^{1/2}$ interpolated to energy E.

4.3. Crossing of Scoring Planes.

A set of scoring planes at depths $z = z_\ell$, $\ell = 1,2,....$, is introduced. It is convenient to define these depths in terms of fractions b_ℓ of the CSDA range r_0 (at the initial energy of the protons). The scaling of depths in units of r_0 minimizes the explicit dependence of dE/dz and y(T,z) on the energy of the incident beam, and makes it easy to choose scoring planes which allow a good description of the Bragg peak of the depth-dose distribution.

The values of b_ℓ should extend from zero to at most 1.04. Penetration beyond this depth is extremely unlikely and of no practical interest. It desirable to space the scoring depths especially closely in the neighborhood of the Bragg peak, which occurs for b_ℓ close to 0.99.

Suppose that the n^{th} step of the condensed random walk involves a crossing of the boundary plane $z = z_\ell$. In other words, $z_n < z_\ell < z_{n+1}$. Let E_n and E_{n+1} denote the corresponding energies, and $\cos\theta_n$ and $\cos\theta_{n+1}$ the corresponding obliquity cosines, before and after the crossing. Let $a = (z_\ell - z_n)/(z_{n+1} - z_n)$ denote the fraction of the step that has been traversed by the proton when the crossing occurs. The energy E_{cr} at the point of crossing is obtained by linear interpolation,

$$E_{cr} = E_n - a(E_n - E_{n+1}) \quad . \tag{4.3.1}$$

The survival factor $W_{cr} = W(E_{cr})$, the nuclear attenuation factor $\mu_{cr} = \mu(E_{cr})$, and the stopping power $S_{cr} = S(E_{cr})$ are obtained by interpolation to energy E_{cr}. The obliquity cosine at the point of crossing is obtained by liner interpolation,

$$\cos\theta_{cr} = \cos\theta_n + a(\cos\theta_{n+1} - \cos\theta_n) \quad . \tag{4.3.2}$$

The radial distance at the point of crossing is calculated as

$$\rho_{cr} = \left[\left(x_n + a(x_{n+1} - x_n)\right)^2 + \left(y_n + a(y_{n+1} - y_n)\right)^2\right]^{1/2} \quad , \tag{4.3.3}$$

4.4. Crossing Scores.

Four scores are recorded for the crossing, which depend on the cosine of the direction of motion, $\cos\theta_{cr}$, and on the nuclear survival weight factor, W_{cr}, and the stopping power S_{cr}, evaluated at the crossing energy E_{cr}:

(1)	$S_{cr}\, W_{cr}/\cos\theta_{cr}$	used to estimate $(dE/dz)_c$, and $f(\rho,z)$;
(2)	$W_{cr}\, \mu_{cr}\, E_{cr}/\cos\theta_{cr}$	used to estimate $(dE/dz)_n$;
(3)	$1/\cos\theta_{cr}$	used to estimate $y(T,z)$;
(4)	$S_{cr}/\cos\theta_{cr}$	used to estimate $S(T)\, y(T,z)$, where $S(T)$ is the stopping power.

(4.4.1)

Actually the absolute value of $\cos\theta_{cr}$ should be used in these scores, but negative values of $\cos\theta_{cr}$ were never encountered in all the runs of PTRAN for beam energies from 250 MeV to 50 MeV. Radial distributions are scored by assigning Score (1) to the appropriate radial histogram bin according the value of ρ_{cr}. Energy spectra are scored by assigning Scores (3) and (4) to the appropriate energy histogram bin according to the value of E_{cr}. Score (4) is not really necessary, because $S(T)\, y(T,z)$ could also be obtained by multiplying the Monte Carlo estimate of $y(T,z)$ with $S(T)$ at the end of the calculation. However, the use of (4) is inherently more accurate.

4.5. Scoring of Track Ends.

When the proton energy E falls below a chosen value E_{cut}, the history is terminated, and the score $E_{cut}\, W(E_{cut})$ is recorded at the appropriate depth interval of a histogram. It has been found that this histogram, as a function of depth, can be represented with sufficient accuracy by a Gaussian distribution. The track-end scores are utilized by a processing program called PTSUM, which is discussed in Section 4.9.

4.6. Input for PTRAN3D.

Input Parameters. The user is prompted to supply the following input data:

NBEG = Grid index that specifies the initial proton energy. The relation between grid indices and energies is given in file PARAM4.TBj for data set j.

NFIN = Grid index for the final proton energy at which the Monte Carlo histories are terminated

IHIST = Number of Monte Carlo histories to be sampled

IMONIT = Number of histories in group; the set of sampled histories is divided into (IHIST/IMONIT) groups. After the completion of each successive group, the number of completed histories is shown on the monitor screen. Results for different groups are used to determine the statistical uncertainties of various quantities.

INRAN = Random number seed for congruential random number generator (should be odd in order not to reduce the period)

BDFIL = Name of the boundary-information file. This file must be prepared in advance, and should contain the following information:

LBMAX, IBMAX	=	Number of scoring depths and radial bins
(BR(L), L=1,LBMAX)	=	Depths of the scoring planes, in units of the CSDA range
(MEMAX(L),L=1,LBMAX)	=	Number of energy bins (of equal size) used to classify proton energy spectra
(EBOT(L), L=1,LBMAX)	=	Lowest energies (MeV) used for spectral energy classification
(ETOP(L), L=1,LBMAX)	=	Highest energies (MeV) used for spectral energy classification.
(RTOP(L), L=1,LBMAX)	=	Largest radial distance (g/cm^2) for classifying the radial distribution of energy loss.

Cases in which the crossing energy E_{cr} is smaller than EBOT or larger than ETOP are not included in the spectrum. Cases in which the radial distance ρ_{cr} at the time of crossing exceeds RTOP are not included in the radial distribution. Appropriate values of the arrays EBOT(L), ETOP(L) and RTOP(L) can be estimated from the results of preliminary results of PTRAN3D. This will be discussed below in Section 4.8.

Options. The user is prompted by the program to decide whether energy-loss straggling, angular multiple-scattering deflections, and spatial multiple-scattering displacements should be included. Except for exploratory model studies, the answer to all three questions should be affirmative. Finally, the user is asked to specify the name of the output file.

Input Arrays. The user must supply the names of three large input files. File names are suggested by the program, but the use of these names is not mandatory:

PDAT: Contains cross sections and parameters, generated by program PARAM4;

VDAT: Contains arrays needed for sampling from the Vavilov energy-loss distribution, generated by program VPREP4;

MDAT: Contains arrays needed for sampling from the Molière multiple scattering distribution, generated by program MPREP4.

Also available must be two auxiliary input files: THSET2 contains a set of reduced angles required for the sampling of angular multiple scattering deflections. GAUSS.DAT contains data used for selecting random variates from a Gaussian distribution, which is required for the sampling of lateral multiple scattering displacements according to Eqs (2.7) and (2.8).

4.7. Output from PTRAN3D.

File Names. The output file starts with a listing of the names of the input files used for PDAT, VDAT, MDAT and BDFIL. Then follows the name of the output file. With this information the user has a complete record of the input data associated with each output file.

Input Parameters and Options. Next follows a listing of various input parameters and options used in the run, including IHIST, INRAN, LBMAX, IBMAX, NBEG, NFIN (described in Section 4.6). In addition, three other parameters are listed which indicate what options were chosen:

ISTRAG = 1: Energy-loss straggling included
2: Energy-loss straggling omitted

IMULT = 1: Multiple-scattering deflections included
2: Multiple-scattering deflections omitted

IREF = 1: Lateral multiple-scattering displacements included
2: Lateral multiple-scattering displacements omitted

Other Pertinent Quantities. Also listed are:

EBEG = Initial energy, MeV, corresponding to index NBEG
EFIN = Final energy, MeV, corresponding to index NFIN
RANGE = CSDA range, g/cm^2, at energy EBEG.

Output Table. The next section of the output file has the form of a table containing the following quantities:

L = Index of scoring plane

BR = Depth of scoring plane, in units of CSDA range;

SCORC = $(dE/dz)_c$, mean energy loss per unit depth, MeV cm^2/g, due to Coulomb interactions with atoms, associated with crossing of the Lth scoring plane

PERCC = Error (percent standard deviation) of SCORC, estimated from the dispersion of the results obtained with (IHIST/IMONIT) groups of histories

SCORN = $(dE/dz)_n$, mean energy loss per unit depth, MeV cm^2/g, due to nonelastic nuclear interactions, associated with the crossing of the Lth scoring plane

PERCN = Error (percent standard deviation) of SCORN, estimated from the dispersion of the results obtained with (IHIST/IMONIT) groups of histories

CROSS = Fraction of proton tracks in the Monte Carlo simulation which crossed the Lth scoring plane. Note that nonelastic interactions do not prevent such crossings, because they are taken into account by means of a survival weight factor.

SCORC, SCORN and CROSS are normalized to one incident proton.

RMAX = Maximum radial distance from beam axis (g/cm^2) with which proton tracks crossed the L'th boundary in the entire Monte Carlo run. RMAX is also stored in an auxiliary output file (see Section 4.8). If RTOP is properly chosen, RMAX is close to and smaller than RTOP.

RTOP = Upper limit (g/cm^2) of the radial distance from the beam axis included in the histogram representing the radial distribution of energy loss

EXCESS = Fraction of the energy loss at the L^{th} scoring depth that involves radial distances greater than RTOP. Pertains to events that are not included in the radial histogram.

EBOT (ETOP) = Lower (upper) energy limit (MeV) of the spectral histogram

EMIN (EMAX) = Minimum (maximum) energy (MeV) with which proton tracks crossed the L'th boundary in the entire Monte Carlo run. EMIN and EMAX are also stored in an auxiliary output file (see Section 4.8). If EBOT is properly chosen, EMIN is close to and larger than EBOT, and EMAX is close to and smaller than ETOP.

MEMAX = Number of spectral energy bins

MLOW (MHIG) = Number of sampled tracks in which a crossing energy occurred that was smaller than EBOT (or larger than ETOP) and was not included in the computation of the energy spectrum

Output Arrays. The part of the output file consists of large arrays for use in other computer calculations that analyze the output of PTRAN3D.

(i) *Energy Losses in Track Ends*

DFSUM: Energy,in MeV (per incident proton) lost in track ends

KRMAX: Number of depth intervals (of equal size) in which the track-end energy losses are scored

ZRMIN, ZRMAX: Minimum and maximum depths (in units of the CSDA range) between which the track-end energy losses are scored

(DUMPF(K), K=1,KRMAX): Track-end energy losses, MeV, in various depth intervals

DFSUM and DUMPF are normalized to one incident proton, and provide input needed by the processing program PTSUM described below in Section 4.6.

(ii) *Track Lengths and Moments of Energy Spectra*

(TRACK(L), L=1,LBMAX) = average track length per unit depth at various depths

(EMOM1(L), L=1,LBMAX) = average proton energy, MeV, at various depths, calculated as track average, from Eq (4.1.1).

(ESIG(L), L=1,LBMAX) = standard deviation of the proton energy, MeV, at various depths, from Eq (4.1.2).

TRACK and EMOM1 are normalized to one incident proton. In the computation of EMOM1 and ESIG all events are included, even the rare events with crossing energies E_{cr} smaller than EBOT or larger than ETOP.

(iii) *Energy Spectra and Radial Distributions*

For each of the LBMAX scoring depths, the following information is given:

First record: L, BR, MEMAX, EBOT,ETOP, IBMAX, RTOP, where

L	=	index of scoring plane
BR	=	depth of scoring plane, in units of CSDA range
MEMAX	=	number of spectral energy bins
EBOT (ETOP)	=	lower (upper) limit of spectral histogram, MeV
IBMAX	=	number or radial bins
RTOP	=	upper limit of radial histogram, g/cm^2

Subsequent records:

(Y(M), M=1,MEMAX) = histogram of y(T,z), track length, per unit depth and energy, in individual energy bins. Units are MeV^{-1}.

(YS(M), M=1,MEMAX) = histogram of S(T)y(T,z), track length multiplied by stopping power, per unit depth and energy. Units are cm^2/g.

(RADC(I),I=1,IBMAX) = fractions of the energy lost in each of the IBMAX radial bins. Results pertain to energy losses due to Coulomb interactions.

The histograms Y(M) and YS(M) are normalized to one incident proton. The widths of the histogram bins is DE = (ETOP-EBOT)/MEMAX. The sum Y(1)+Y(2)...+Y(MEMAX), multiplied by DE, is equal the track length per unit depth, TRACK(L), listed previously in the output file. The sum YS(1)+YS(2)+...YS(MEMAX), multiplied by DE, is equal to the contribution to $(dE/dz)_c$ from scoring-plane crossings.

The histogram RADC(I) is normalized so that the sum RADC(1)+RADC(2)+... +RADC(IBMAX) + EXCESS(L) is equal to unity. The width of the histogram bins is DR = RTOP/IBMAX. In terms of the radial distribution function,

$$\text{RADC(I)} = 2\pi \int_{R_1}^{R_2} \rho \; f(\rho,z)\, d\rho \quad , \tag{4.7.1}$$

where R_1 = (I-1)*DR and R_2 = I*DR.

Timing. The last two items of the output file consist of:

Elapsed time for the run, in minutes
Dates and times at the beginning and end of the run.

This information is also displayed at the end of the run on the monitor screen, followed by the name of the output file.

4.8. *Auxiliary Output File.*

An auxiliary output file is automatically written, whose name is the same as that of the regular output file, preceded by X. This file contains the EMIN, EMAX and RMAX arrays for all the crossing boundaries. The arrays obtained in a preliminary run of PTRAN3D can be used as estimates for the arrays EBOT,ETOP and RTOP, and can be inserted into the boundary crossing file BDFIL.

4.9. *Program PTSUM: Combination of Crossing and Track End Scores*

A processing program, PTSUM, uses the output file from PTRAN3D to calculate the total energy loss $(dE/dz)_c$ due to Coulomb interactions (practically equal to energy deposition $(dD/dz)_n$ by combining the scores from scoring-boundary crossings and from track ends. PTSUM also checks the accuracy of the calculation, by verifying that $(dE/dz)_c + (dE/dz)_n$, integrated over all depths, equals the energy with which the proton enters the medium. The output from PTSUM is stored in two files: a summary table, and a file with arrays useful for further computer calculations. Table 3 presents a typical summary file, for the case of a 160-MeV proton beam. The contents of the second output file are as follows:

Name of input file from PTRAN3D
Name of output file from PTSUM
Beam energy T_0 (MeV), and CSDA range r_0 (g/cm^2) at energy T_0

LMAX	=	number of scoring depths
(BR(L),L=1,LMAX)	=	set of scoring depths (in units of r_0)
(SCORCT(L),L=1,LMAX)	=	set of values of $(dE/dz)_c$
(SCORN(L),L=1,LMAX)	=	set of values of $(dE/dz)_n$
(DF(L),L=1,LMAX)	=	contributions to $(dE/dz)_c$ from track ends

Tables 4 and 5 list results obtained with PTSUM for proton beams with seven energies between 250 MeV and 50 MeV. Table 4 shows the fractional contribution from track ends to $(dE/dz)_c$, as a function of depth, and Table 5 gives the ratio $(dE/dz)_n$ /$(dE/dz)_c$ of nuclear to Coulomb energy losses, again as a function of depth.

5. Monte Carlo Program PTRAN1D

PTRAN1D is a one dimensional version of PTRAN3D, which omits the treatment of the radial distribution of deposited energy. Again, a narrow pencil beam is assumed to be incident along the z-axis. However, because of the omission of the radial variable ρ, results obtained with PTRAN1D can be interpreted as applying to a broad parallel incident beam.

In the one-dimensional treatment involving only the variable z, the azimuthal angle φ is irrelevant, and the changes of azimuthal angle according to Eqs (2.4) and (2.5) need not be evaluated. Moreover, the lateral spatial multiple-scattering displacements are quite unimportant. Therefore, Eqs (2.5) and (2.6) are not used, the sampling of k_x and k_y from a Gaussian distribution is avoided, and it is assumed that $\Delta x' = \Delta y' = 0$. It has been verified that the error incurred thereby is negligible in regard to $(dE/dz)_c$, $(dE/dz)_n$ and y(T,z). As a result of these simplifications, runs of PTRAN1D take only about 2/3 of the time needed with PTRAN3D.

PTRAN1D requires the same input files PDAT, VDAT and MDAT as PTRAN3D. The boundary input file BDFIL can also be the same as that used with PTRAN3D, but the parameter IBMAX and the array RTOP, pertaining to the radial distribution, can be omitted. The auxiliary input file GAUSS.DAT is not required.

The output from PTRAN1D has the same format and content as that from PTRAN3D, except that the radial energy-loss distributions RADC are omitted. The processing program PTSUM can also be applied to the output from PTRAN1D.

6. Random Numbers

Congruential Generator. The random numbers needed in PTRAN3D and PTRAN1D are obtained by a congruential generator, which is coded in-line and requires only two statements, and is therefore very fast:

```
IR=IAND(MASK,IR*MULT)
R=RNORM*IR
```

IR is a random integer. R is the corresponding real random number (between 0 and 1) from a uniform distribution, obtained with normalizing factor RNORM = 2^{-31} = 4.656612873E-10. MASK has the decimal value 2147483647, which corresponds to a binary number 0111 1111 1111 1111 1111 1111 1111 1111. The operator IAND, applied to the product IR*MULT, makes the most significant bit of IR zero. The multiplier MULT should be chosen so that there is a minimum amount of correlation between successive numbers in the pseudo-random number sequence. The period of the sequence can be shown to be $2^{29} \cong 5.37E+08$. The initial value of IR (the random number seed) should be an odd integer; otherwise, the period will be shortened.

Tests with program PTRAN1D, using step-size Grid 4, indicated that approximately 1500 random numbers were required for sampling a single proton track from an initial energy of 160 MeV down to 140 keV. Thus the period of the random number generator is such that only 358,000 histories can be generated before the sequence of random numbers repeats itself.

In PTRAN3D and PTRAN1D, two sequences of random numbers are actually used: IRA (with a multiplier MULTA = 69069) and IRB (with a multiplier MULTB = 1664525). According to Knuth (1981) these multipliers give rise to sequences which have a satisfactory lack of correlation, as indicated by the theoretical spectral test. An IRB sequence is used to provide random number seeds for successive proton histories. Within each history random numbers from an IRA sequence are used.

With this procedure one can generate approximately 537 million histories each of which has a different starting random number seed. One cannot guarantee that there are no repetitions and overlaps between the random-numbers sets for different histories generated with the multiplier MULTA. It seems very unlikely, however, that such repetitions will occur often enough so that they could significantly influence the Monte Carlo results. The best way to reassure oneself is to make comparisons with calculations in which random numbers are generated by a different generator with a longer period.

Fibonacci Generator. An alternative version of PTRAN1D, called PTRAN1DX, uses a random number generator due to Marsaglia and Zaman (1987). This generator is based on a Fibonacci sequence, and is stated to satisfy stringent empirical tests of randomness. The generator has the very long period $2^{44} = 1.79E13$. In PTRAN1DX a subroutine RANMAR from James (1988) is used, which is an adaptation of the Marsaglia-Zaman generator and generates random numbers in batches of 1000, thereby reducing the time expended on calls to the subroutine. There is also an initializing subroutine RMARIN which requires two input numbers as seeds.

Several numerical experiments were carried out comparing results for the same problem obtained with PTRAN1D and PTRAN1DX. No statistically significant differences were found in regard to $(dE/dz)_c$, $(dE/dz)_n$, and y(T,z). However, the required computing time was about 1/3 higher for PTRAN1DX than for PTRAN1D.

Use of Intrinsic Random-Number Generating Function. Many Fortran compilers provide an intrinsic function that generates uniform random numbers, usually by the multiplicative congruential method. As a convenience for users who would like to use such an intrinsic function, another version of PTRAN1D, called PTRAN1DY, was prepared. In this version random numbers are assumed to be generated by an intrinsic function RND, and the random number sequence is started by an intrinsic function RANDS(x), where x (a real number between 0 and 1) is the random number seed.

7. Influence of Step-Size Grid

Runs of program PTRAN1D, for a proton beam energy with an initial energy of 160 MeV, were made with five step-size grids, as described in Section 3.1. The grid parameter ΔT and the computing times for sampling (and scoring) 1 million Monte Carlo histories down to an energy of 140 keV was as follows:

Grid	ΔT (MeV)	Time (Minutes)	Relative Time
1	4	162	1.0
2	2	190	1.17
3	1	263	1.62
4	0.5	475	2.93
5	0.25	750	4.63

These runs were made using a personal computer with a 25 Mhz 486 processor and a Weitek 4167 coprocessor.

In regard to the quantity $(dE/dz)_c$ the differences between the results obtained with different grids were small: less than 0.1 percent for depths $z < 0.9\ r_0$; less than 1 percent for $0.9\ r_0 < z < 1.01\ r_0$, and less than 3 percent for $z = 1.02\ r_0$.

Larger differences were found in regard to the track-length distribution y(T,z). Figs. 3, 4 and 5 , for depths $z = 0.1\ r_0$, $0.5\ r_0$, and $0.9\ r_0$, respectively, for a beam energy of 160 MeV, shows the percentage amounts by which y(T,z) obtained with Grid 2, Grid 3, or Grid 4 differs from the value obtained with Grid 5. The differences are 1 to 3 percent in the central region of the spectrum, but are considerably larger in the wings of the spectrum.

Comparison runs were also made of radial distributions calculated with program PTRAN3D, with Grids 1, 2, 3, and 4. Results are shown in Figs.6 and 7 for a 160-MeV beam of protons, at a depth $z = 0.1\ r_0$. In addition to the Monte Carlo histograms, smooth curves are shown which represent the radial distribution calculated from the theory of Molière (1955), with energy-loss taken into account in the continuous-slowing-down approximation.

The Monte Carlo results in figure 6 were obtained without taking into account the spatial multiple-scattering displacements, i.e., setting $\Delta x' = \Delta y' = 0$ in Eq (2.10). It can be seen that the finer the grid the closer the histograms approach the curve from the Molière theory. In figure 7 a similar set of results is shown, which were obtained with the lateral multiple-scattering displacements included. In this case there is little variation from one grid to another.

It is interesting that the Monte Carlo results obtained with Grid 4 (in fig. 6) or with all grids (in fig. 7), agree well with the curve from the Molière theory. Similar agreement was also obtained at other depths. The implication is that the use of PTRAN3D is not really necessary, but could be replaced by the combined use of PTRAN1D and the Molière theory. Of course this could only be done for depths smaller than the CSDA range. Beyond the Bragg peak the PTRAN3D program is still needed.

8. Program and Data Files

Users can obtain from the author of this report a 3.5 inch, 1.44 Mb disk with four archive files, named PARAM.EXE, VPREP.EXE, MPREP.EXE and PTRAN.EXE. The contents of these files are listed in table 7. The archive files are self-extracting. For example, by running the program PARAM one recovers all the individual files stored in the archive file PARAM.EXE.

Included among the files in VPREP.EXE and MPEP.EXE are the formatted files VPREP4.ARj and MPREP4.ARj, j = 2,3,4, but not the corresponding binary files VPREP4.BRj and MPREP4.BRj which are needed to run PTRAN1D or PTRAN3D. The reason for this omission is that binary files are in general not portable, and depend on the type of computer, and on the compiler used. The user can easily generate the binary files with the VCON4 and MCON4 programs.

Appendix 1. Molière Distribution

According to the theory of Molière (1948), the distribution of multiple-scattering angular deflections can be expressed as a unique function of a scaled angular variable ϑ:

$$F_M(\vartheta)\,\vartheta d\,\vartheta = \vartheta d\vartheta \left[e^{-\vartheta^2} + \frac{f^{(1)}(\vartheta)}{B} + \frac{f^{(2)}(\vartheta)}{B^2} + \cdots \right] . \qquad \text{(A1.1)}$$

The relation between the scaled angle ϑ and the actual multiple-scattering deflection angle θ is

$$\vartheta = \frac{\theta}{\chi_c \sqrt{B}} , \qquad \text{(A1.2)}$$

where χ_c and B are functions of the particle energy and the path length Δs.

Molière's theory was developed in the small-angle approximation, and is applicable when the multiple scattering angles θ are no greater than approximately 20 degrees. In the present application to protons this is not a significant restriction. The expansion in inverse powers of B in Eq (A1.1) is accurate only when B is larger than about 4.5. As discussed by Molière, the use of additional terms in the expansion would not significantly increase the accuracy, because of approximations made elsewhere in the derivation of theory.

The expansion coefficients in Eq (A1.1) are given by

$$f^{(n)}(\vartheta) = \frac{1}{n!} \int_0^\infty y\,dy\; J_0(\vartheta y)\; e^{-y^2/4} \left[\frac{y^2}{4} \log \frac{y2}{4} \right]^n , \qquad \text{(A1.3)}$$

when J_0 denotes a Bessel function.

The quantities $f^{(1)}$ and $f^{(2)}$ were first tabulated by Molière (1948), and later by Bethe (1953) and Scott (1963). In the course of the present work an even more extensive table of coefficients was calculated. This table includes values of $f^{(1)}$ and $f^{(2)}$ at 131 values of ϑ between 0 and 2.6, and 331 values of $\vartheta^4 f^{(1)}$ and $\vartheta^4 f^{(2)}$ at 331 values of ϑ between 2.4 and 60.0. The new results are contained in the files MOLC1.COF and MOLC2.COF distributed with the PTRAN programs.

For a compound, χ_c^2 is obtained as a sum over the corresponding quantities for the atomic constituents:

$$\chi_c^2 = \sum_j w_j\, \chi_{cj}^2 , \qquad \text{(A1.4)}$$

where w_j is the fraction by weight of the j^{th} atomic constituent, and

$$\chi_{cj}^2 = 4\pi N_a \left[r_e \frac{m}{M} \frac{\tau+1}{\tau(\tau+2)} \right]^2 \frac{Z_j^2}{A_j} \Delta s \quad . \tag{A1.5}$$

Here N_a is the Avogadro constant, Z_j and A_j are the atomic number and atomic weight of the j^{th} constituent, r_e is the classical electron radius, m/M is the electron-proton mass ratio, τ is the proton kinetic energy in units of the proton rest mass, and Δs is the path length.

The Molière parameter B depends on the ratio of the characteristic angle χ_c to a screening angle χ_a, and is obtained from the equation

$$B - \log B = \log (\chi_c/\chi_a)^2 + 1 - 2\gamma \quad , \tag{A1.6}$$

where $\gamma = 0.5772156649...$ is Euler's constant. This equation can be easily solved iteratively by Newton's method.

The screening angle χ_a is given by

$$\log \chi_a^2 = \left(1/\chi_c^2\right) \sum_j w_j \chi_{cj}^2 \left[\log \chi_{aj}^2 - F_j/Z_j \right] \quad , \tag{A1.7}$$

with

$$\chi_{aj}^2 = \left[\frac{m}{M} \frac{\alpha}{k_{TF}} \right]^2 k_{HF} \left[1.13 + 3.76 \left(Z_j \alpha/\beta \right)^2 \right] \frac{Z_j^{2/3}}{\tau(\tau+2)} \quad . \tag{A1.8}$$

Here $k_{TF} = (9\pi^2)^{1/3} 2^{-7/3} = 0.88534...$ is a constant associated with the Thomas-Fermi model, α is the fine-structure constant and β is the proton velocity in units of the velocity of light. The quantity in square brackets in Eq (A1.8) is an approximation obtained by Molière with a Thomas-Fermi potential. The correction factor k_{HF} (which depends on $Z_j\alpha/\beta$) converts the screening angle to one corresponding to a Hartree-Fock potential, and was calculated by Berger and Wang (1988), using a formulation of Molière's theory given by Zeitler and Olsen (1964). Values of k_{HF} for selected elements are given in table 8.

The term F_j/Z_j in Eq (A1.7) is an addition to Molière's theory, due to Fano (1956), that takes into influence of the orbital electrons. F_j is given by

$$F_j = \log \left[1130 \beta^2 Z_j^{-4/3} (1-\beta^2)^{-1} \right] - u_j - \beta^2/2 \quad , \tag{A1.6}$$

where the constant u_j has value -3.6 for hydrogen and -5.1 for oxygen.

Appendix 2. Vavilov Distribution

The distribution of energy losses from the theory of Vavilov (1957), $F_V(\lambda,\beta,\kappa)$, is a function of a scaled energy-loss variable λ, and also depends – more weakly – on β and on a skewness parameter κ defined below. For small κ, the Vavilov distribution approaches the Landau distribution (Landau, 1944), whereas for large κ it approaches a Gaussian distribution.

The relation between the scaled energy-loss λ and the energy loss Δ is

$$\lambda = \frac{\Delta - \Delta_{av}}{\xi} + \lambda_{av} \quad , \tag{A2.1}$$

where Δ_{av} is the average energy loss, and

$$\xi = 2\pi r_e^2 mc^2 \frac{\Delta s}{\beta^2} \sum_j w_j \frac{Z_j}{A_j} \quad . \tag{A2.2}$$

Here r_e is the classical electron radius, mc^2 the electron rest energy, and Z_j, A_j, and w_j are the atomic number, atomic weight and fraction by weight of the j^{th} atomic constituent. The quantity λ_{av} in Eq (A2.1) is

$$\lambda_{av} = -1 + \gamma - \beta^2 - \log \kappa \quad , \tag{A2.3}$$

where $\gamma = 0.5772156649...$ is Euler's constant. The skewness parameter κ is

$$\kappa = \frac{\xi}{E_M} \quad , \tag{A2.4}$$

where

$$E_M = \frac{2mc^2 \beta^2}{1 - \beta^2} \quad , \tag{A2.5}$$

is the maximum amount of energy which a proton can lose in a collision with an orbital electron (considered as free).

The quantity ξ has the following significance. In a path length Δs, there will occur, on the average, one collision with an orbital electron in which the proton loses an amount of energy greater than ξ. The Vavilov distribution is accurate under two conditions: (1) the path length must be long enough so that ξ is much greater than the mean excitation energy of the material (75 eV for water); (2) The path length must be short enough so that the mean energy loss Δ_{av} is small compared to the initial proton energy.

The formula for the Vavilov distribution is

$$F_V(\lambda,\beta,\kappa)\,d\lambda = \frac{d\lambda}{\pi}\,\kappa e^{\kappa(1+\beta^2\gamma)} \int_0^\infty \exp\left[h_1(y)\right]\cos\left[h_2(y)\right]dy \quad , \tag{A2.6}$$

where

$$h_1(y) = \kappa\left[f_1(y) - \frac{\epsilon}{2}\,y^2\left(1-\beta^2/2\right)\right] \quad , \tag{A2.7}$$

$$h_2(y) = \kappa\left[y(\lambda + \log\kappa) + f_2(y)\right] \quad , \tag{A2.8}$$

$$f_1(y) = \beta^2\left[\log y - \mathrm{Ci}(y)\right] - \cos y - y\,\mathrm{Si}(y) \quad , \tag{A2.9}$$

$$f_2(y) = y\left[\log y - \mathrm{Ci}(y)\right] + \sin y + \beta^2\,\mathrm{Si}(y) \quad , \tag{A2.10}$$

$$\mathrm{Si}(y) = \int_0^y \frac{\sin t}{t}\,dt \qquad \text{(sine integral)} \quad , \tag{A2.11}$$

$$\mathrm{Ci}(y) = \gamma + \log y - \int_0^y \frac{\cos t}{t}\,dt \qquad \text{(cosine integral)} \quad . \tag{A2.12}$$

Efficient methods for evaluating the sine and cosine integrals by series expansions and rational approximations can be found in Abramowitz and Stegun (1964).

The quantity ϵ in Eq (A2.7) is a binding correction which was applied Blunck and Leisegang (1951) to Landau's theory and by Shulek *et al.* (1959) to Vavilov's theory. As shown by Fano (1963) the variance, Ω^2, of the energy-loss distribution is

$$\Omega^2 = \xi\,E_M\left(1-\beta^2/2\right)(1+\epsilon) \quad , \tag{A2.13}$$

with

$$\epsilon = \frac{2S_1}{E_M(1-\beta^2/2)}\,\log\left[\frac{2mc^2\beta^2}{I_1}\right] \quad . \tag{A2.14}$$

S_1 and I_1 are averages taken over the oscillator strength distribution:

$$S_1 = \int_0^\infty E \frac{df}{dE} dE \quad , \tag{A2.15}$$

$$\log I_1 = \frac{1}{S_1} \int_0^\infty E \log(E) \frac{df}{dE} dE \quad , \tag{A2.16}$$

where df/dE is the density of optical dipole oscillator strength per unit excitation energy, E, above the ground state. In the present work, experimental values for these quantities were used, from a compilation of Zeiss *et al.* (1977): $S_1 = 191.2$ eV, $I_1 = 939.9$ eV. These values were obtained for water vapor, but is expected that their use for liquid water will cause little error. With these input data one obtains the following values of ϵ:

Energy (MeV) =	200	100	50	20	10	5.13	3.97
ϵ =	0.00554	0.00973	0.0168	0.0238	0.0553	0.0849	0.0984

Straggling measurements by Besenbacher *et al.* (1981) for protons in low-Z gases suggest that at low energies Eq (A2.14) overestimates Ω^2. In the present work, Eq (A2.14) was therefore used only down to an energy where ϵ reaches a limiting value $\epsilon_{lim} = 0.1$. Below that energy, ϵ was kept constant.

References

Abramowitz, M. and Stegun, I. A. (1964). *Handbook of Mathematical Functions*, National Bureau of Standards Applied Mathematics Series 55.

Berger, M. J. (1963). Monte Carlo calculation of the penetration and diffusion of charged particles. In Methods in Computational Physics, Vol. 1, p. 135, Academic Press, N.Y.

Berger, M. J. (1992). *ESTAR, PSTAR and ASTAR: Computer Codes for Calculating Stopping Power and Range Tables for Electrons, Protons and Helium Ions*, National Institute of Standards and Technology Report NISTIR 4999.

Berger, M. J. and Wang, R. (1988). Multiple-scattering angular deflections and energy-loss straggling. Chapter 2, p. 21, in *Monte Carlo Transport of Electrons and Photons* (Eds. T.M. Jenkins, W.R. Nelson, and A. Rindi), Plenum Press, N.Y.

Besenbacher, F., Andersen, H. H., Hvelplund, P., and Knudsen, H. (1981). Straggling in energy loss of swift hydrogen and helium ions in gases, Kgl. Danske VIdenskab. Selskab. Mat.-Fys. Medd. **40**, No.3.

Bethe, H. A. (1953). Molière's theory of multiple scattering, Phys. Rev. **89**, 1256.

Blunck, O. and Leisegang, S. (1950). Zum Energieverlust schneller Elektronen in dunnen Schichten, Z. Phys. **128**, 500.

Carlson, R. F., Cox, A. J., Nimmo, J. R., Davison, N. E., Elbakr, S. A., Horton, J. L., Houdayer, A., Sourkes, A. M., van Oers, W.T.H., and Margazkotis, D. J. (1975). Proton total reaction cross sections for the doubly magic nuclei ^{16}O, ^{40}Ca, and ^{208}Pb in the energy range 20-50 MeV, Phys. Rev. **C12**, 1167.

Fano, U. (1963). Penetration of protons, alpha particles and mesons, Ann. Rev. Nucl. Sci. **13**, 1.

ICRU (1992). *Stopping Powers and Ranges for Protons and Alpha Particles*, Report 49, in press, International Commission on Radiation Units and Measurements, Bethesda, MD.

James, D. (1988). A review of pseudorandom number generators, CERN Data Handling Division, Report DD/88/22.

Kahaner, D., Moler, C. and Nash, S (1989). *Numerical Methods and Software*, Prentice-Hall (Englewood Cliffs, N.J.).

Knuth, D. E. (1981). The Art Of Computer Programming, Vol.2, Seminumerical Algorithms, Addison-Wesley (Reading, MA).

Kronmal, R. A. and Peterson, Jr., A. V. (1979). On the alias method for generating random variables, The Amer. Statistian, **33**, 214. Also, unpublished memorandum, Programs for generating discrete random integers using Walker's alias method.

Landau, L. (1944). On the energy loss of fast particles by ionization, J. Phys. USSR **8**, 201.

Marsaglia, G. and Zaman, A.(1987). Toward a universal random number generator, Florida State University Report FSU-SCRI-87-50.

Molière, G. (1948). Theorie der Streuung schneller geladener Teilchen II. Mehrfach- und Vielfachstreuung, Z. Naturforschung **3a**, 78.

Molière, G. (1955). Theorie der Streuung schneller geladener Teilchen III. Die Vielfachstreuung von Bahnspuren unter Berucksichtigung der statistischen Kopplung, Z. Naturforschung **10a**, 177.

Renberg, P. U., Measday, D. F., Pepian, M., Savier, B., and Richard-Sarre, C. (1972). Reaction cross sections for protons in the energy region 220 to 570 MeV, Nucl. Phys. **A183**, 81.

Scott, W. T. (1963). The theory of small-angle multiple-scattering of fast charged particle, Rev. Mod. Phys. **35**, 231.

Shulek, P., Golovin, B. M., Kulyukina, L. A., Medved, S. V., and Pavlovich, P. (1966). Fluctuations of ionization loss, Yad. Fiz. **4**, 564. (Engl. transl. Sov. J. Nucl. Phys. **4**, 400, 1967).

Vavilov, P. V. (1957). Ionization losses of high-energy particles, Zh. Eksp. Teor. Fiz. **32**, 920 (Engl. transl. Sov. Phys. JETP **5**, 749, 1957).

Walker, A. J. (1974). Fast generation of uniformly distributed pseudorandom numbers with floating point representation, Electronics Letters **10**, 553.

Young, P. G., Arthur, E. D., Bozoian, M., England, T. R., Hale, G. M., LaBauve, R. J., Little, R. C., MacFarlane, R. E., Madland, D. G., Perry, R. T., and Wilson, W. B. (1990). Transport Data Libraries for Incident Proton and Neutron Energies to 100 MeV. Los Alamos National Laboratory Publication LA-11753-MS.

Zeitler, E. and Olsen, H. (1964). Screening effects in elastic electron scattering, Phys. Rev. **136A**, 1546.

Table 1. Proton stopping powers and ranges in water. Calculated assuming a mean excitation energy I = 75 eV.

T = Proton energy, MeV
STOP(e) = electronic stopping power, MeV cm^2/g
STOP(n) = nuclear stopping power, MeV cm^2/g
STOP(t) = total stopping power, MeV cm^2/g
RANGE(c) = CSDA range, cm^2/g
RANGE(p) = projected range, cm^2/g
DETOUR = detour factor = RANGE(c)/RANGE(p)

T	STOP(e)	STOP(n)	STOP(t)	RANGE(c)	RANGE(p)	DETOUR
0.1000	8.145E+02	1.620E+00	8.161E+02	1.607E-04	1.458E-04	0.9073
0.2000	6.604E+02	9.016E-01	6.613E+02	2.966E-04	2.806E-04	0.9460
0.3000	5.497E+02	6.351E-01	5.504E+02	4.631E-04	4.462E-04	0.9635
0.4000	4.714E+02	4.928E-01	4.719E+02	6.599E-04	6.422E-04	0.9731
0.5000	4.128E+02	4.043E-01	4.132E+02	8.869E-04	8.683E-04	0.9790
0.6000	3.676E+02	3.438E-01	3.680E+02	1.144E-03	1.124E-03	0.9829
0.8000	3.037E+02	2.658E-01	3.039E+02	1.745E-03	1.724E-03	0.9877
1.0000	2.606E+02	2.173E-01	2.608E+02	2.458E-03	2.435E-03	0.9905
2.0000	1.585E+02	1.157E-01	1.586E+02	7.555E-03	7.519E-03	0.9952
3.0000	1.171E+02	7.972E-02	1.172E+02	1.499E-02	1.494E-02	0.9965
4.0000	9.398E+01	6.113E-02	9.404E+01	2.458E-02	2.451E-02	0.9971
5.0000	7.906E+01	4.970E-02	7.911E+01	3.623E-02	3.613E-02	0.9974
6.0000	6.854E+01	4.195E-02	6.858E+01	4.984E-02	4.972E-02	0.9976
8.0000	5.456E+01	3.208E-02	5.460E+01	8.277E-02	8.259E-02	0.9978
10.0000	4.564E+01	2.603E-02	4.567E+01	1.230E-01	1.228E-01	0.9980
15.0000	3.290E+01	1.778E-02	3.292E+01	2.539E-01	2.535E-01	0.9982
20.0000	2.605E+01	1.356E-02	2.607E+01	4.260E-01	4.252E-01	0.9983
30.0000	1.875E+01	9.239E-03	1.876E+01	8.853E-01	8.839E-01	0.9984
40.0000	1.487E+01	7.034E-03	1.488E+01	1.489E+00	1.486E+00	0.9985
50.0000	1.244E+01	5.691E-03	1.245E+01	2.227E+00	2.224E+00	0.9985
60.0000	1.078E+01	4.786E-03	1.078E+01	3.093E+00	3.089E+00	0.9986
70.0000	9.555E+00	4.134E-03	9.559E+00	4.080E+00	4.075E+00	0.9986
80.0000	8.622E+00	3.641E-03	8.625E+00	5.184E+00	5.176E+00	0.9986
90.0000	7.884E+00	3.255E-03	7.888E+00	6.398E+00	6.389E+00	0.9986
100.0000	7.286E+00	2.944E-03	7.289E+00	7.718E+00	7.707E+00	0.9987
110.0000	6.791E+00	2.689E-03	6.794E+00	9.140E+00	9.128E+00	0.9987
120.0000	6.374E+00	2.475E-03	6.377E+00	1.066E+01	1.065E+01	0.9987
130.0000	6.018E+00	2.294E-03	6.021E+00	1.228E+01	1.226E+01	0.9987
140.0000	5.711E+00	2.137E-03	5.713E+00	1.398E+01	1.396E+01	0.9987
150.0000	5.443E+00	2.001E-03	5.445E+00	1.577E+01	1.576E+01	0.9987
160.0000	5.207E+00	1.882E-03	5.209E+00	1.765E+01	1.763E+01	0.9988
170.0000	4.997E+00	1.777E-03	4.999E+00	1.961E+01	1.959E+01	0.9988
180.0000	4.810E+00	1.683E-03	4.812E+00	2.165E+01	2.163E+01	0.9988
190.0000	4.642E+00	1.598E-03	4.644E+00	2.377E+01	2.374E+01	0.9988
200.0000	4.491E+00	1.522E-03	4.492E+00	2.596E+01	2.593E+01	0.9988
210.0000	4.353E+00	1.453E-03	4.354E+00	2.822E+01	2.819E+01	0.9988
220.0000	4.227E+00	1.390E-03	4.229E+00	3.055E+01	3.052E+01	0.9988
230.0000	4.112E+00	1.332E-03	4.114E+00	3.295E+01	3.291E+01	0.9988
240.0000	4.007E+00	1.279E-03	4.008E+00	3.541E+01	3.537E+01	0.9988
250.0000	3.910E+00	1.231E-03	3.911E+00	3.794E+01	3.790E+01	0.9989

Table 2. Excerpts from output file PARAM4.TB4, generated by program PARAM4.

TSTEP	NSTEP1	TFAC	NSTEP2
0.50	492	0.95000	82

N = index number of track segment
T = energy at beginning of segment, MeV
TAV = energy at midpoint of segment, MeV
STEP = path length of track segment, g/cm^2
STOPAV = stopping power at midpoint of segment, MeV cm^2/g
CHIC = ch(subc), deg
CHIA = ch(suba), deg
COL = (CHIC/CHIA)**2 = average number of collisions
B = Molière parameter B
SCALE = ch(subc)*sqrt(B), deg
SCALE1 = (pi/180) ch(subc)*sqrt((B-1.2)/6)
ATTNUC = nuclear (nonelastic) attenuation coefficient, cm^2/g
SURV = survival probability (non-elastic nuclear)

N	T	TAV	STEP	STOPAV	CHIC	CHIA	COL	B	SCALE	SCALE1	ATTNUC	SURV
11	250.00000	249.75000	1.27815E-01	3.91192E+00	3.47450E-02	3.73074E-04	8.67350E+03	1.13421E+01	1.17015E-01	7.88422E-04	9.57968E-03	9.87759E-01
111	200.00000	199.75000	1.11254E-01	4.49422E+00	3.97594E-02	4.29999E-04	8.54959E+03	1.13263E+01	1.33809E-01	9.01504E-04	9.73777E-03	8.79890E-01
211	150.00000	149.75000	9.17578E-02	5.44913E+00	4.71842E-02	5.15062E-04	8.39219E+03	1.13060E+01	1.58654E-01	1.06878E-03	1.00263E-02	7.95807E-01
311	100.00000	99.75000	6.84958E-02	7.29972E+00	5.98661E-02	6.62391E-04	8.16834E+03	1.12763E+01	2.01032E-01	1.35405E-03	1.08420E-02	7.32211E-01
411	50.00000	49.75000	4.00239E-02	1.24925E+01	8.96020E-02	1.01829E-03	7.74270E+03	1.12176E+01	3.00101E-01	2.02069E-03	1.37476E-02	6.85918E-01
471	20.00000	19.75000	1.89964E-02	2.63206E+01	1.53160E-01	1.83805E-03	6.94349E+03	1.10979E+01	5.10230E-01	3.43335E-03	1.78843E-02	6.66910E-01
491	10.00000	9.75000	1.07347E-02	4.65774E+01	2.32009E-01	2.99375E-03	6.00592E+03	1.09383E+01	7.67329E-01	5.15882E-03	1.24833E-02	6.63593E-01
504	5.13342	5.00509	3.24923E-03	7.89932E+01	2.48033E-01	4.98943E-03	2.47126E+03	9.95625E+00	7.82632E-01	5.22962E-03	0.00000E+00	6.63267E-01
522	2.03907	1.98809	6.40422E-04	1.59195E+02	2.76779E-01	1.11938E-02	6.11380E+02	8.38810E+00	8.01614E-01	5.28740E-03	0.00000E+00	6.63267E-01
536	0.99440	0.96954	1.86749E-04	2.66236E+02	3.06312E-01	2.25138E-02	1.85111E+02	7.01450E+00	8.11264E-01	5.26286E-03	0.00000E+00	6.63267E-01
549	0.51047	0.49771	6.16533E-05	4.13983E+02	3.42765E-01	4.44508E-02	5.94612E+01	5.66524E+00	8.15842E-01	5.16085E-03	0.00000E+00	6.63267E-01
567	0.20277	0.19770	1.52788E-05	6.63548E+02	4.29506E-01	1.16861E-01	1.35082E+01	3.77809E+00	8.34844E-01	4.91383E-03	0.00000E+00	6.63267E-01

N = index number of track segment
T = energy at beginning of segment, MeV
BQ = beta**2 at beginning of track segment
STEP = path length of track segment, g/cm^2
DAV = average energy loss in segment MeV
VAR = variance of energy loss in segment, MeV**2
EPS = Blunck-Leisegang correction included in VAR
DELT2 = 0.5*EPS/(1-0.5 BQ), term in Vavilov integral
XSI = straggling parameter xsi, MeV
XSIRAT = ratio of xsi to mean excitation energy
WMAX = maximum energy loss in single collisions, MeV
KAPPA = Vavilov parameter kappa

N	T	BQ	STEP	DAV	VAR	EPS	DELT2	XSI	XSIRAT	WMAX	KAPPA
11	250.00000	3.7652E-01	1.2781E-01	5.0000E-01	1.4561E-02	4.5979E-03	1.8662E-03	2.8932E-02	3.8576E+02	6.1717E-01	4.6878E-02
111	200.00000	3.2054E-01	1.1125E-01	5.0000E-01	1.2042E-02	5.5376E-03	2.3250E-03	2.9581E-02	3.9441E+02	4.8213E-01	6.1355E-02
211	150.00000	2.5667E-01	9.1758E-02	5.0000E-01	9.4378E-03	7.0122E-03	3.0561E-03	3.0468E-02	4.0624E+02	3.5289E-01	8.6339E-02
311	100.00000	1.8335E-01	6.8496E-02	5.0000E-01	6.7004E-03	9.7320E-03	4.4199E-03	3.1839E-02	4.2452E+02	2.2946E-01	1.3876E-01
411	50.00000	9.8627E-02	4.0024E-02	5.0000E-01	3.7388E-03	1.6849E-02	8.0090E-03	3.4586E-02	4.6115E+02	1.1183E-01	3.0928E-01
471	20.00000	4.1306E-02	1.8996E-02	5.0000E-01	1.7474E-03	3.3819E-02	1.6560E-02	3.9195E-02	5.2260E+02	4.4034E-02	8.9012E-01
491	10.00000	2.0980E-02	1.0735E-02	4.9999E-01	9.9732E-04	5.5344E-02	2.7382E-02	4.3608E-02	5.8144E+02	2.1901E-02	1.9911E+00
504	5.13342	1.0853E-02	3.2492E-03	2.5667E-01	3.0874E-04	8.4940E-02	4.2239E-02	2.5515E-02	3.4020E+02	1.1214E-02	2.2754E+00
522	2.03907	4.3323E-03	6.4042E-04	1.0195E-01	6.1493E-05	1.0000E-01	4.9892E-02	1.2599E-02	1.6798E+02	4.4469E-03	2.8331E+00
536	0.99440	2.1163E-03	1.8675E-04	4.9719E-02	1.7912E-05	1.0000E-01	4.9947E-02	7.5207E-03	1.0028E+02	2.1674E-03	3.4699E+00
549	0.51047	1.0872E-03	6.1653E-05	2.5523E-02	5.9103E-06	1.0000E-01	4.9973E-02	4.8330E-03	6.4440E+01	1.1123E-03	4.3449E+00
567	0.20277	4.3207E-04	1.5279E-05	1.0138E-02	1.4642E-06	1.0000E-01	4.9989E-02	3.0138E-03	4.0184E+01	4.4177E-04	6.8221E+00

Table 3. Sample output from program PTSUM.

Input file: PTRAN3D.TST
Output file: PTSUM.TST

PARTITION OF ENERGY LOSS IN ENTIRE PHANTOM:

```
(a) Initial proton energy: 160.000 MeV
(b) Energy lost in Coulomb interactions: 141.929 MeV
      Contribution from boundary crossing scores:1 141.813 MeV
      Contribution to from track ends:   0.116 MeV
(c) Energy lost in non-elastic nuclear interactions:  18.064 MeV
(d) Sum of (b) and (c): 159.993 MeV
```

PARTITION OF ENERGY LOSS AT VARIOUS DEPTHS:

```
    z/r = depth in units of CSDA range
          r = 1.765E+01 g/cm2
C(cross) = Coulomb interactions, crossing of scoring boundaries
  C(end) = Coulomb interactions, track ends
       C = C(cross)+C(end)
       N = non-elastic nuclear interactions
```

Average Energy Loss per Unit Depth, MeV cm2/g

z/r	C(cross)	C(end)	C	N	C+N	C(end)/C	N/(C+N)
0.000	5.207	0.000	5.207	1.592	6.798	0.00000	0.23413
0.100	5.333	0.000	5.333	1.483	6.816	0.00000	0.21761
0.200	5.491	0.000	5.491	1.375	6.866	0.00000	0.20026
0.300	5.692	0.000	5.692	1.267	6.959	0.00000	0.18205
0.400	5.952	0.000	5.952	1.158	7.111	0.00000	0.16291
0.450	6.113	0.000	6.113	1.104	7.217	0.00000	0.15297
0.500	6.300	0.000	6.300	1.049	7.350	0.00000	0.14276
0.550	6.522	0.000	6.522	0.994	7.516	0.00000	0.13228
0.600	6.787	0.000	6.787	0.939	7.726	0.00000	0.12150
0.650	7.112	0.000	7.112	0.882	7.994	0.00000	0.11036
0.700	7.520	0.000	7.520	0.824	8.344	0.00000	0.09877
0.720	7.714	0.000	7.714	0.800	8.515	0.00000	0.09397
0.740	7.932	0.000	7.932	0.776	8.707	0.00000	0.08907
0.760	8.177	0.000	8.177	0.750	8.927	0.00000	0.08406
0.780	8.455	0.000	8.455	0.724	9.180	0.00000	0.07890
0.800	8.776	0.000	8.776	0.697	9.473	0.00000	0.07360
0.820	9.150	0.000	9.150	0.669	9.819	0.00000	0.06811
0.840	9.593	0.000	9.593	0.639	10.232	0.00000	0.06241
0.860	10.131	0.000	10.131	0.606	10.737	0.00000	0.05645
0.880	10.801	0.000	10.801	0.571	11.372	0.00000	0.05020
0.900	11.668	0.000	11.668	0.532	12.201	0.00000	0.04364
0.910	12.210	0.000	12.210	0.512	12.722	0.00000	0.04025
0.920	12.854	0.000	12.854	0.491	13.345	0.00000	0.03679
0.930	13.638	0.000	13.638	0.468	14.107	0.00000	0.03320
0.940	14.625	0.000	14.625	0.443	15.068	0.00000	0.02939
0.950	15.930	0.000	15.930	0.412	16.342	0.00000	0.02523
0.955	16.772	0.000	16.772	0.394	17.166	0.00000	0.02295
0.960	17.795	0.000	17.795	0.373	18.168	0.00002	0.02051
0.965	19.117	0.001	19.119	0.347	19.466	0.00007	0.01784
0.970	20.875	0.006	20.881	0.317	21.198	0.00027	0.01496
0.975	23.075	0.018	23.093	0.281	23.374	0.00078	0.01202
0.980	25.802	0.047	25.849	0.238	26.086	0.00181	0.00912
0.985	28.353	0.098	28.452	0.189	28.641	0.00345	0.00660
0.990	29.549	0.166	29.714	0.138	29.853	0.00557	0.00463
0.995	27.866	0.224	28.090	0.091	28.181	0.00799	0.00322
1.000	23.525	0.245	23.769	0.052	23.821	0.01029	0.00218
1.005	16.679	0.214	16.893	0.026	16.919	0.01268	0.00151
1.010	9.919	0.151	10.070	0.011	10.081	0.01499	0.00104
1.015	4.874	0.085	4.960	0.003	4.963	0.01723	0.00070
1.020	1.860	0.039	1.899	0.001	1.900	0.02049	0.00049
1.025	0.546	0.014	0.560	0.000	0.560	0.02543	0.00036
1.030	0.130	0.004	0.134	0.000	0.134	0.03123	0.00022
1.035	0.016	0.001	0.017	0.000	0.017	0.05746	0.00058
1.040	0.004	0.000	0.004	0.000	0.004	0.04319	0.00000

Table 4. Fraction of energy loss (in Coulomb interactions) due to track ends, as function of depth in units of CSDA range, z/r_0, for proton beams incident with energy T_0.

T_0, MeV	250.0	200.0	160.0	130.0	100.0	70.0	50.0
r_0, g/cm^2	37.94	25.96	17.65	12.28	7.718	4.080	2.227
z/r_0				F R A C T I O N			
0.950	0.00000	0.00000	0.00000	0.00000	0.00000	0.00000	0.00001
0.955	0.00000	0.00000	0.00000	0.00000	0.00001	0.00002	0.00004
0.960	0.00001	0.00001	0.00002	0.00003	0.00004	0.00009	0.00018
0.965	0.00003	0.00005	0.00008	0.00011	0.00018	0.00034	0.00060
0.970	0.00013	0.00019	0.00028	0.00039	0.00058	0.00100	0.00166
0.975	0.00043	0.00059	0.00080	0.00106	0.00152	0.00245	0.00383
0.980	0.00108	0.00142	0.00186	0.00238	0.00325	0.00499	0.00745
0.985	0.00217	0.00276	0.00351	0.00439	0.00583	0.00861	0.01247
0.990	0.00362	0.00452	0.00563	0.00693	0.00903	0.01301	0.01854
0.995	0.00525	0.00646	0.00795	0.00972	0.01255	0.01785	0.02499
1.000	0.00690	0.00844	0.01034	0.01255	0.01607	0.02263	0.03147
1.005	0.00855	0.01038	0.01265	0.01533	0.01957	0.02746	0.03831
1.010	0.01018	0.01228	0.01502	0.01817	0.02307	0.03232	0.04446
1.015	0.01209	0.01447	0.01764	0.02122	0.02668	0.03733	0.05134
1.020	0.01430	0.01694	0.02043	0.02462	0.03133	0.04300	0.05947
1.025	0.01716	0.02059	0.02440	0.02890	0.03698	0.05058	0.06755
1.030	0.02197	0.02632	0.03148	0.03551	0.04471	0.05934	0.07954
1.035	0.03446	0.03256	0.04153	0.04684	0.05531	0.07092	0.09662

Table 5. Energy loss from nuclear interactions, as fraction of the energy loss from Coulomb interactions, as function of depth in units of the CSDA range, z/r_0, for proton beams incident with energy T_0.

T_0, MeV	250.0	200.0	160.0	130.0	100.0	70.0	50.0
r_0, g/cm^2	37.94	25.96	17.65	12.28	7.718	4.080	2.227
z/r_0				F R A C T I O N			
0.000	0.61257	0.43368	0.30570	0.22122	0.14880	0.08914	0.05524
0.100	0.55653	0.39407	0.27809	0.20180	0.13644	0.08204	0.05079
0.200	0.50000	0.35411	0.25037	0.18233	0.12398	0.07477	0.04623
0.300	0.44281	0.31380	0.22253	0.16279	0.11137	0.06730	0.04162
0.400	0.38489	0.27320	0.19458	0.14316	0.09852	0.05957	0.03695
0.500	0.32621	0.23235	0.16650	0.12338	0.08530	0.05151	0.03214
0.600	0.26689	0.19125	0.13827	0.10319	0.07154	0.04313	0.02696
0.700	0.20700	0.14986	0.10956	0.08217	0.05695	0.03454	0.02112
0.800	0.14653	0.10773	0.07941	0.05959	0.04123	0.02504	0.01433
0.900	0.08363	0.06196	0.04559	0.03437	0.02371	0.01297	0.00637
0.950	0.04739	0.03514	0.02583	0.01881	0.01182	0.00546	0.00207
0.980	0.01940	0.01366	0.00916	0.00597	0.00318	0.00098	0.00011
0.990	0.01068	0.00725	0.00463	0.00286	0.00137	0.00031	0.00002
1.000	0.00556	0.00362	0.00218	0.00125	0.00052	0.00008	0.00000
1.010	0.00299	0.00184	0.00104	0.00055	0.00018	0.00002	0.00000
1.020	0.00171	0.00097	0.00051	0.00024	0.00006	0.00000	0.00000
1.030	0.00097	0.00059	0.00023	0.00010	0.00003	0.00000	0.00000
1.035	0.00146	0.00066	0.00000	0.00000	0.00000	0.00000	0.00000

Table 6. Comparison of the average energy loss (due to Coulomb interactions) per unit depth, (dE/dz)c, calculated with Grids 1, 2, 3, 4 and 5. The results are for a 160-MeV beam in water, and for each case are based on a sample of 1 million Monte Carlo histories.

z/r_0	$(dE/dz)_c$ MeV cm^2/g	Std.Dev. (Percent)	Difference w.r.t. Grid 5 (Percent)			
(1)	(2)	(3)	(4) Grid 1	(5) Grid 2	(6) Grid 3	(7) Grid 4
0.50	6.300	<0.01	0.01	0.01	0.01	<0.01
0.90	11.667	<0.01	0.06	0.08	0.05	0.03
0.95	15.926	0.01	0.10	0.14	0.11	0.07
0.99	29.459	0.10	0.47	-0.18	0.14	-0.03
1.00	23.435	0.16	0.28	-0.19	-0.60	-0.06
1.01	9.981	0.30	-0.97	-1.29	-2.02	-0.71
1.02	1.891	0.78	-1.42	-2.48	-2.70	-1.54

Column (1): Depth in units of CSDA range r_0. At 160 MeV, $r_0 = 17.65$ g/cm^2.
Column (2): Average energy loss per unit depth due to Coulomb interactions, calculated with Grid 5. Track-end contribution is omitted.
Column (3): Percent standard deviation of results in column (2).
Columns (4) to (7): Percent differences of results calculated with Grids 1, 2, 3 and 4, respectively, from results in column (2) calculated with Grid 5.

Table 7. List of files stored on the 1.44-Mb distribution disk. The files are contained in four self-extracting archive files, PARAM.EXE, VPREP.EXE, MPREP.EXE and PTRAN.EXE.

PARAM.EXE	Self-extracting archive file; expands to 1005408 bytes.
PARAM4.FOR	Fortran source code
COMPOS.WAT	Composition data for water
STOPRANG.WAT	Stopping-power and range table for water
OXFIT.DAT	Total nonelastic nuclear cross section for oxygen
PARAM4.TB1	Output table, Grid 1
PARAM4.TB2	Output table, Grid 2
PARAM4.TB3	Output table, Grid 3
PARAM4.TB4	Output table, Grid 4
PARAM4.TB5	Output table, Grid 5
PARAM4.AR2	Output array for VPREP4 and MPREP4, Grid 2
PARAM4.AR3	Output array for VPREP4 and MPREP4, Grid 3
PARAM4.AR4	Output array for VPREP4 and MPREP4, Grid 4
PARAM4.PT2	Output array for PTRAN1D, PTRAN1DX or PTRAN3D, Grid 2
PARAM4.PT3	Output array for PTRAN1D, PTRAN1DX or PTRAN3D, Grid 3
PARAM4.PT4	Output array for PTRAN1D, PTRAN1DX or PTRAN3D, Grid 4
VPREP.EXE	Self-extracting archive file; expands to 3670457 bytes.
VPREP4.FOR	Fortran source code
VCON4.FOR	Fortran source code
VSAMP4.FOR	Fortran source code
VSUM4.FOR	Fortran source code
VPREP4.AR2	Output file for VCON4, Grid 2
VPREP4.AR3	Output file for VCON4, Grid 3
VPREP4.AR2	Output file for VCON4, Grid 4
	VCON4 produces output files VPREP4.BR2, VPREP4.BR3 or VPREP4.BR4 for use in PTRAN3D or PTRAN1D.
MPREP.EXE	Self-extracting archive file; expands to 2953884 bytes.
MPREP4.FOR	Fortran source code
MCON4.FOR	Fortran source code
MSAMP4.FOR	Fortran source code
THSET2	Reduced deflection angles for Moliere distribution
MOLC1.COF	Moliere expansion coefficients f(1)
MOLC2.COF	Moliere expansion coefficients f(2)
MPREP4.AR2	Output file for MCON4, Grid 2
MPREP4.AR3	Output file for MCON4, Grid 3
MPREP4.AR4	Output file for MCON4, Grid 4
	MCON4 produces output files MPREP4.BR2, MPREP4.BR3 or MPREP4.BR4 for use in PTRAN3D or PTRAN1D.
PTRAN.EXE	Self-extracting archive file; expands to 310428 bytes.
PTRAN3D.FOR	Fortran source code
THSET2	Reduced deflection angles for Moliere distribution
GAUSS.DAT	Arrays used for sampling from Gaussian distribution
PTRAN3D.TST	Output from test run
XPTRAN3D.TST	Auxiliary output from test run
PTRAN1D.FOR	Fortran source code
PTRAN1DX.FOR	Fortran source code
PTRAN1DY.FOR	Fortran source code
PTSUM.FOR	Fortran source code
PTSUMTAB.TST	Output table from test run
PTSUMARR.TST	Output arrays from test run

Table 8. Multiplicative correction factor k_{HF} used in Eq (A1.8). Values in parentheses were obtained by interpolation. This table corrects misprints in Table 2.2 of Berger and Wang (1988).

	Thomas-Fermi Potential	Hartree-Fock Potentials								
$Z\alpha/\beta$		Z = 1	2	4	6	7	8	13	29	47
0.00	1.037	0.863	1.530	1.129	1.058	1.081	1.116	1.186	1.101	1.183
0.05	(1.034)	0.861	1.527	1.127	(1.055)	1.078	1.114	1.183	1.098	1.180
0.1	1.028	0.855	1.517	1.119	1.048	1.071	1.106	1.175	1.091	1.172
0.2	1.004	0.836	1.482	1.094	1.024	1.047	1.081	1.149	1.066	1.145
0.4	0.950	0.790	1.401	1.034	0.969	0.990	1.022	1.086	1.008	1.083
0.6	0.918	0.764	1.355	1.000	0.937	0.957	0.989	1.050	0.975	1.047
0.8	0.912	0.759	1.346	0.994	0.931	0.951	0.982	1.043	0.969	1.040
1.0	0.918	0.764	1.356	1.001	0.937	0.957	0.989	1.050	0.975	1.047
1.2	0.929	0.773	1.371	1.012	0.947	0.968	1.000	1.062	0.986	1.059
2.4	0.968	0.805	1.428	1.054	0.986	1.008	1.041	1.106	1.027	1.102
4.8	0.983	0.818	1.450	1.070	1.001	1.023	1.057	1.122	1.041	1.117
9.6	0.987	0.821	1.454	1.072	1.003	1.025	1.058	1.123	1.040	1.113

Figures

Fig. 1. Total nonelastic nuclear cross sections for protons incident on oxygen-16. The curve represents the cross section used in PTRAN. The experimental points are from Renberg *et al.* (1972) and Carlson *et al.* (1975).

Fig. 2. Vavilov energy-loss distributions for protons in water. Results were calculated for initial energies and path lengths from Grid 4 (see Section 2.2). The various parameters have the following values:

Energy (MeV)	Path Length (g/cm^2)	ξ (MeV)	β^2	κ
25	0.02282	0.03780	0.05123	0.6878
50	0.04002	0.03459	0.09863	0.3093
100	0.06850	0.03184	0.1834	0.1388
200	0.1113	0.02958	0.3205	0.06135

Fig. 3. Dependence of proton energy spectra on the step-size grid used in PTRAN. The bottom panel shows the track-length distribution differential in energy, y(T,z), from a 160-MeV proton beam in water, at a depth $z = 0.1\ r_0$, where r_0 is the CSDA range (17.65 g/cm^2). This histogram was calculated with step-size Grid 5. The top panel shows the percentage amounts by which values of y(T,z) calculated with Grids 2, 3 and 4 differ from the results obtained with Grid 5.

Fig. 4. Similar to Fig. 3, for a depth $z = 0.5\ r_0$.

Fig. 5. Similar to Fig. 3, for a depth $z = 0.9\ r_0$.

Fig. 6. Radial distribution of energy loss due to Coulomb interactions, as a function of the radial distance ρ from a pencil beam, at a depth $z = 0.1\ r_0$, for a 160 MeV beam in water. The histograms represent Monte Carlo results obtained with program PTRAN3D, assuming various step-size grids. The curve is calculated using the theory of Molière (1955), evaluated in the continuous-slowing-down approximation. The Monte Carlo results were obtained taking into account multiple-scattering angular deflections, but neglecting lateral multiple-scattering displacements within each step.

Fig. 7. Similar to Fig. 7, but calculated with inclusion of lateral multiple-scattering displacement in each step.

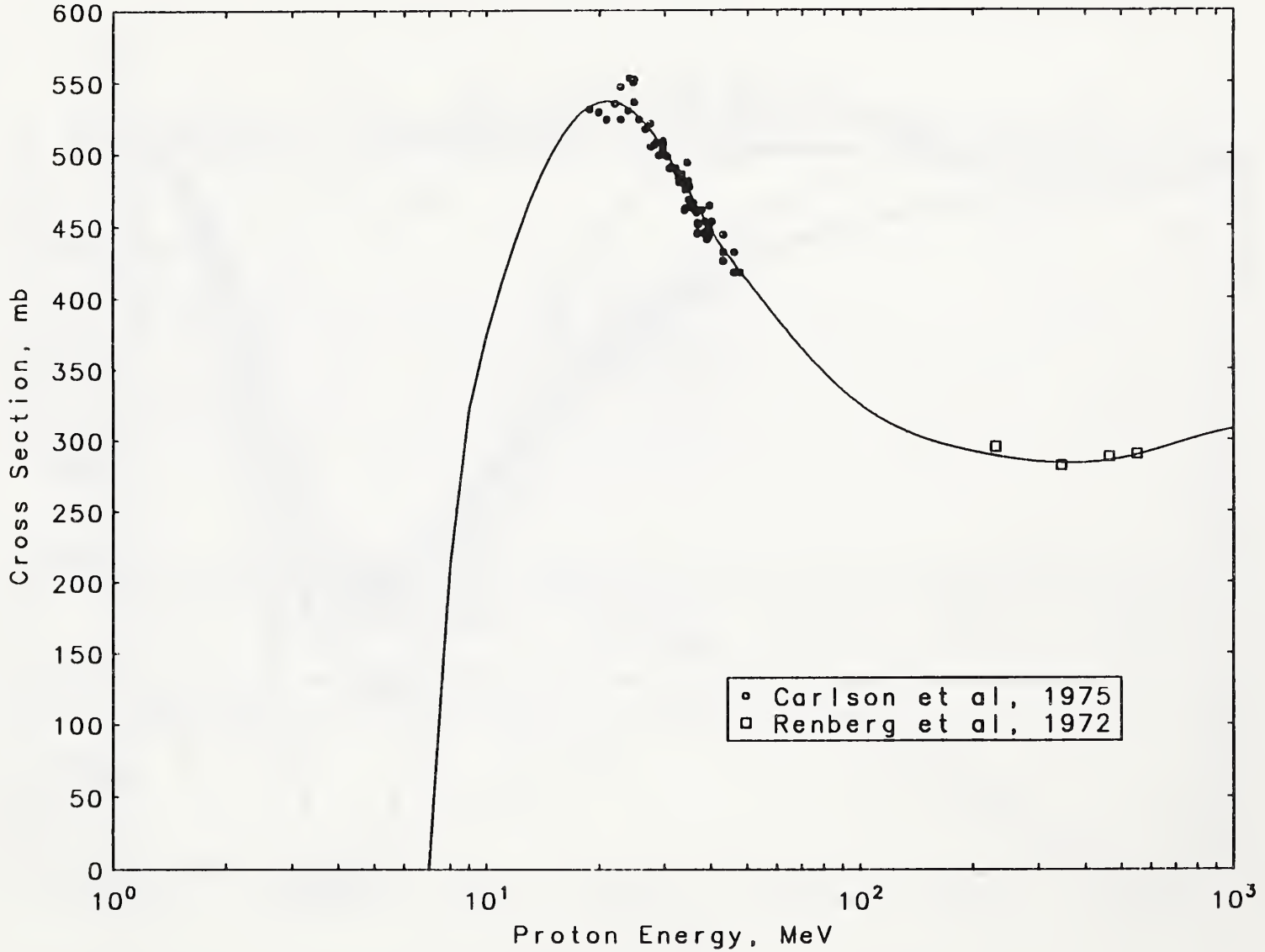
600
550
500
450
400
350
300
250
200
150
100
50
0
Cross Section, mb
10^0
10^1
10^2
10^3
Proton Energy, MeV
Carlson et al, 1975
Renberg et al, 1972

Fig. 1

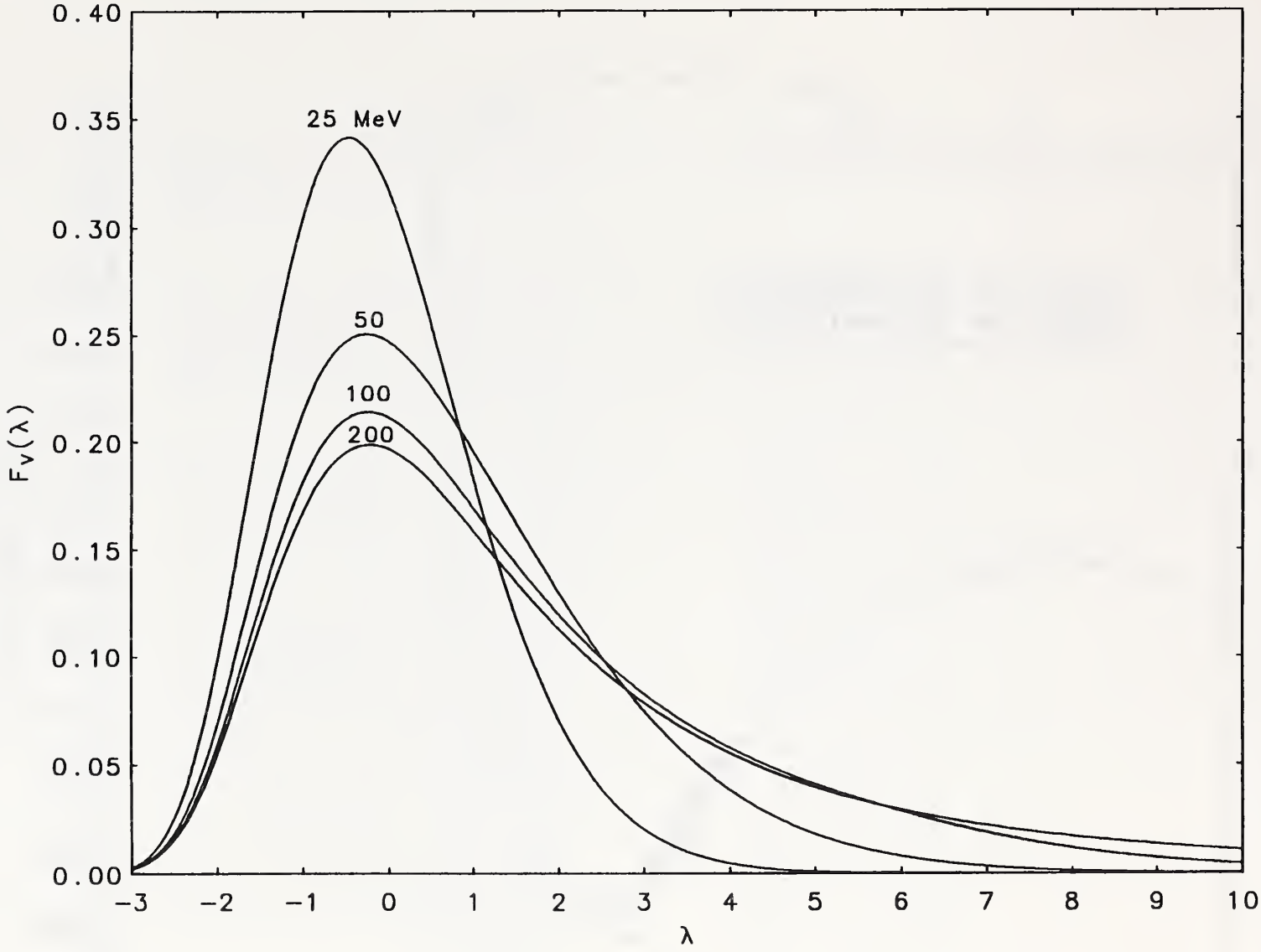
0.40
0.35
0.30
0.25
0.20
0.15
0.10
0.05
0.00
$F_v(\lambda)$
25 MeV
50
100
200
−3
−2
−1
0
1
2
3
4
5
6
7
8
9
10
λ

Fig. 2

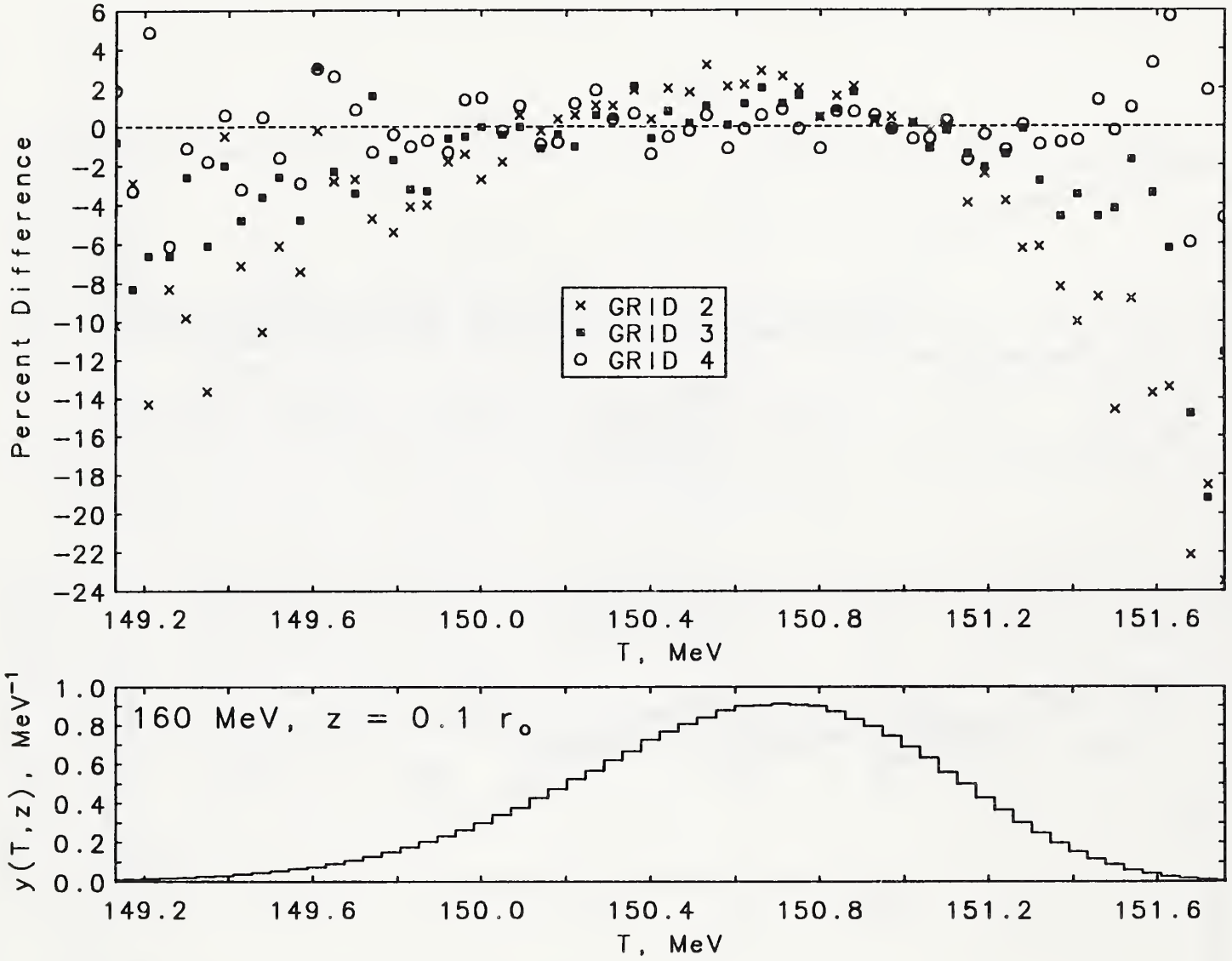
Percent Difference
6
4
2
0
−2
−4
−6
−8
−10
−12
−14
−16
−18
−20
−22
−24
GRID 2
GRID 3
GRID 4
149.2
149.6
150.0
150.4
150.8
151.2
151.6
T, MeV
y(T,z), MeV⁻¹
1.0
0.8
0.6
0.4
0.2
0.0
160 MeV, z = 0.1 r₀
149.2
149.6
150.0
150.4
150.8
151.2
151.6
T, MeV

Fig. 3

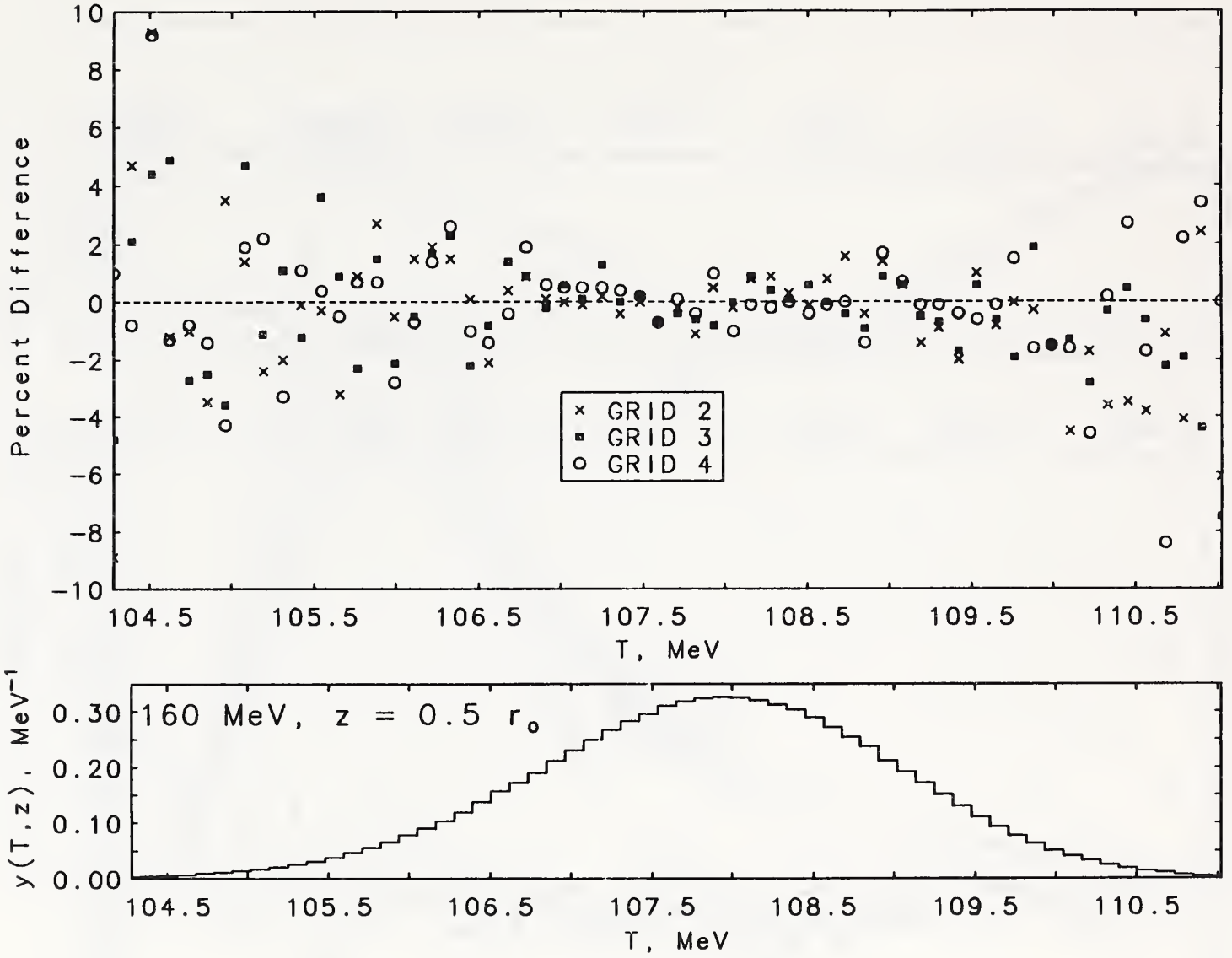
Percent Difference
10
8
6
4
2
0
−2
−4
−6
−8
−10
104.5
105.5
106.5
107.5
108.5
109.5
110.5
T, MeV
GRID 2
GRID 3
GRID 4
y(T,z), MeV⁻¹
0.30
0.20
0.10
0.00
160 MeV, z = 0.5 r₀
104.5
105.5
106.5
107.5
108.5
109.5
110.5
T, MeV

Fig. 4

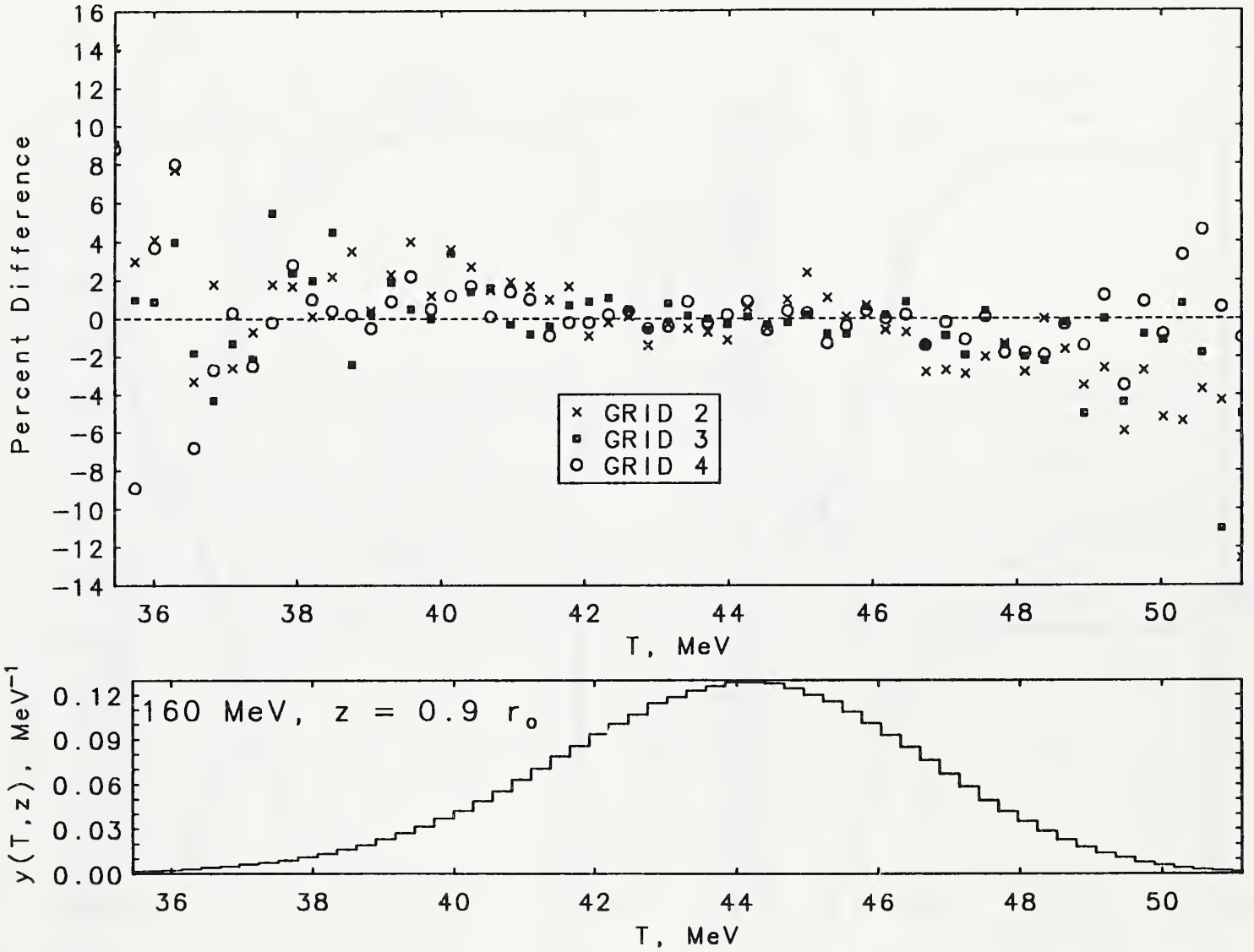
Percent Difference
16
14
12
10
8
6
4
2
0
−2
−4
−6
−8
−10
−12
−14
36
38
40
42
44
46
48
50
T, MeV
× GRID 2
▪ GRID 3
○ GRID 4
y(T,z), MeV⁻¹
0.12
0.09
0.06
0.03
0.00
160 MeV, z = 0.9 r₀
36
38
40
42
44
46
48
50
T, MeV

Fig. 5

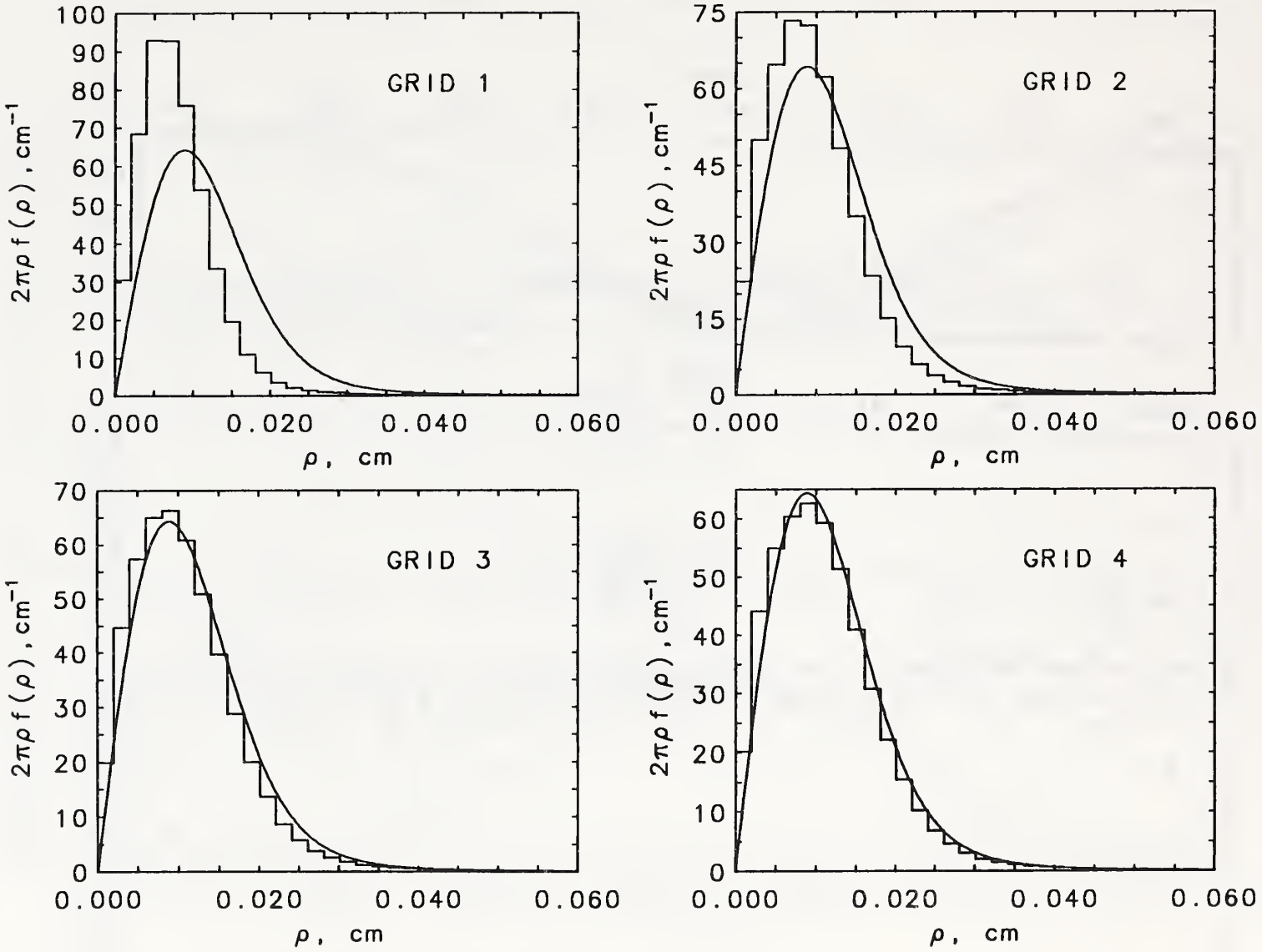

Fig. 6

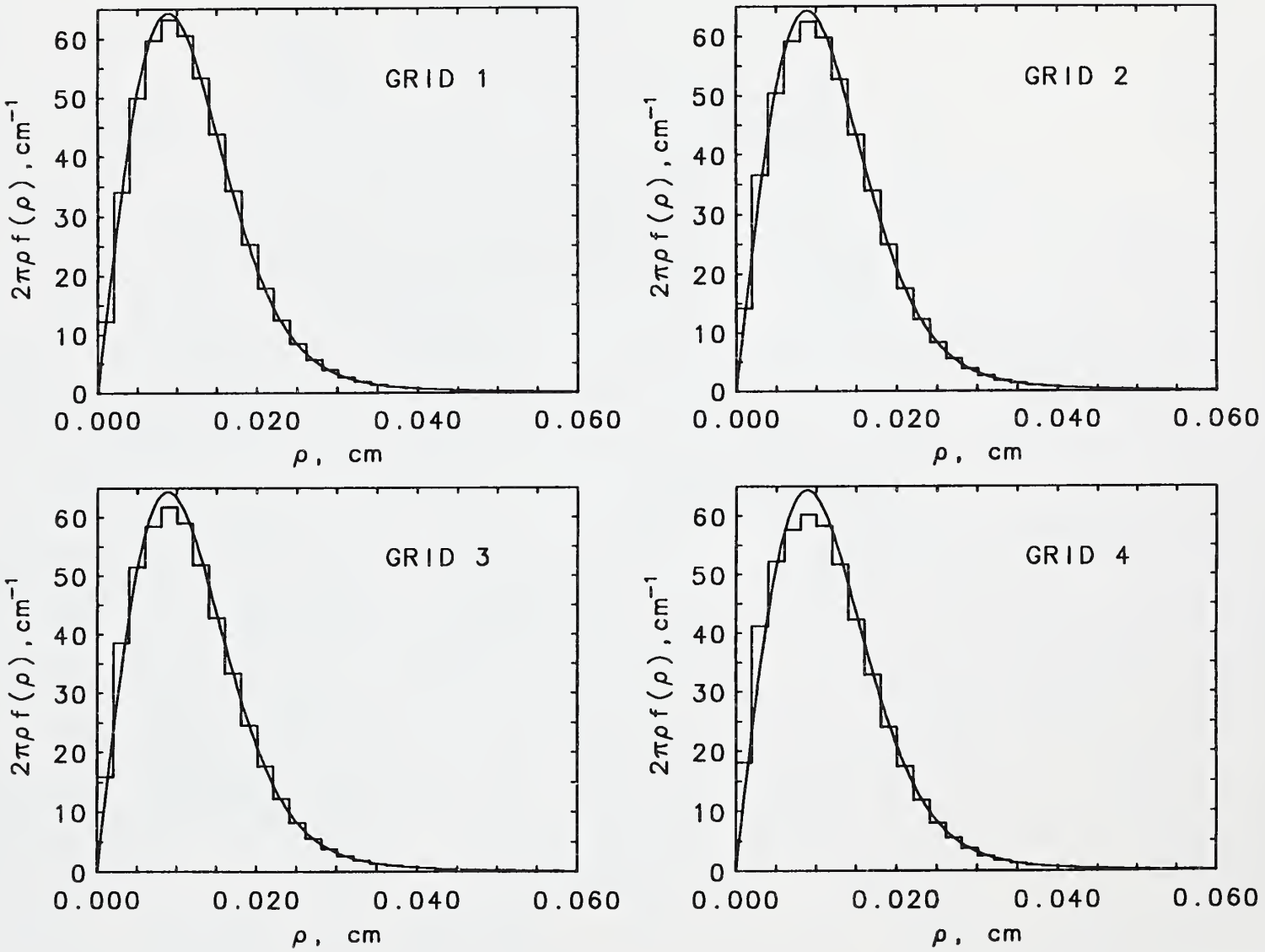
GRID 1
GRID 2
GRID 3
GRID 4
$2\pi\rho f(\rho)$, cm^{-1}
ρ, cm
0
10
20
30
40
50
60
0.000
0.020
0.040
0.060

Fig. 7